



This is a repository copy of *Mapping hidden residual structure within the Myc bHLH-LZ domain using chemical denaturant titration*.

White Rose Research Online URL for this paper:
<https://eprints.whiterose.ac.uk/149959/>

Version: Accepted Version

Article:

Panova, S., Cliff, M.J., Macek, P. et al. (6 more authors) (2019) Mapping hidden residual structure within the Myc bHLH-LZ domain using chemical denaturant titration. *Structure*, 27 (10). 1537-1546.e4. ISSN 0969-2126

<https://doi.org/10.1016/j.str.2019.07.006>

Article available under the terms of the CC-BY-NC-ND licence
(<https://creativecommons.org/licenses/by-nc-nd/4.0/>).

Reuse

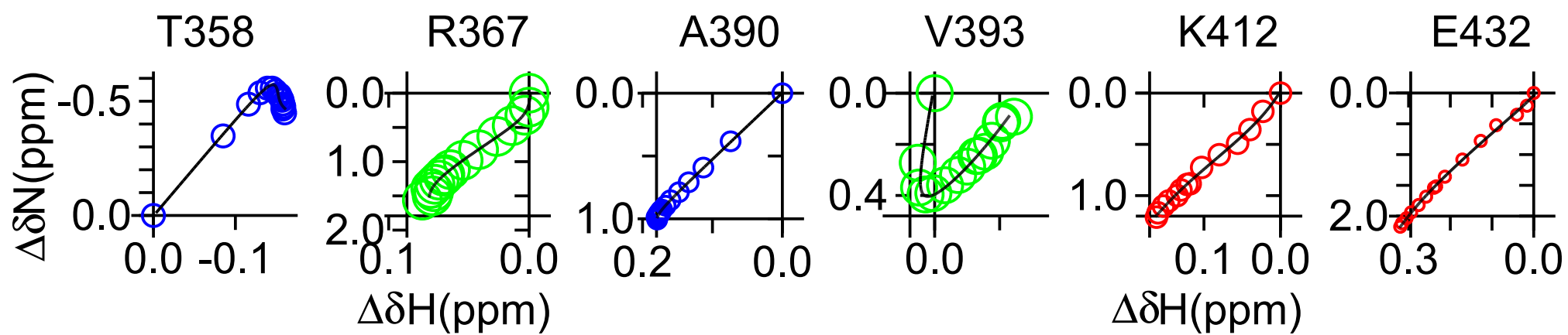
This article is distributed under the terms of the Creative Commons Attribution-NonCommercial-NoDerivs (CC BY-NC-ND) licence. This licence only allows you to download this work and share it with others as long as you credit the authors, but you can't change the article in any way or use it commercially. More information and the full terms of the licence here: <https://creativecommons.org/licenses/>

Takedown

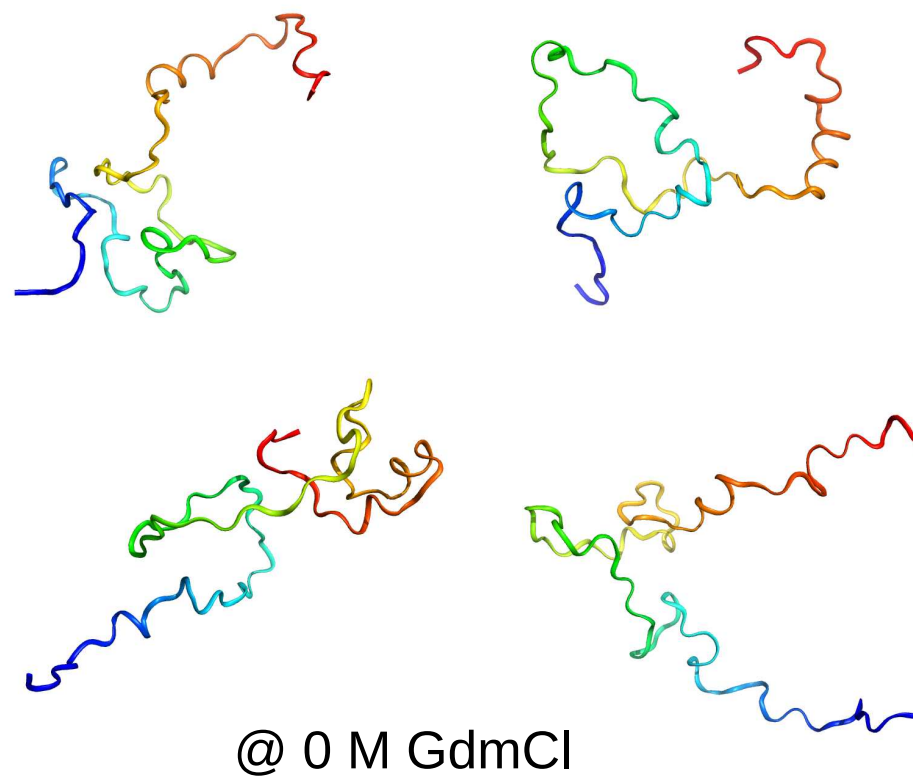
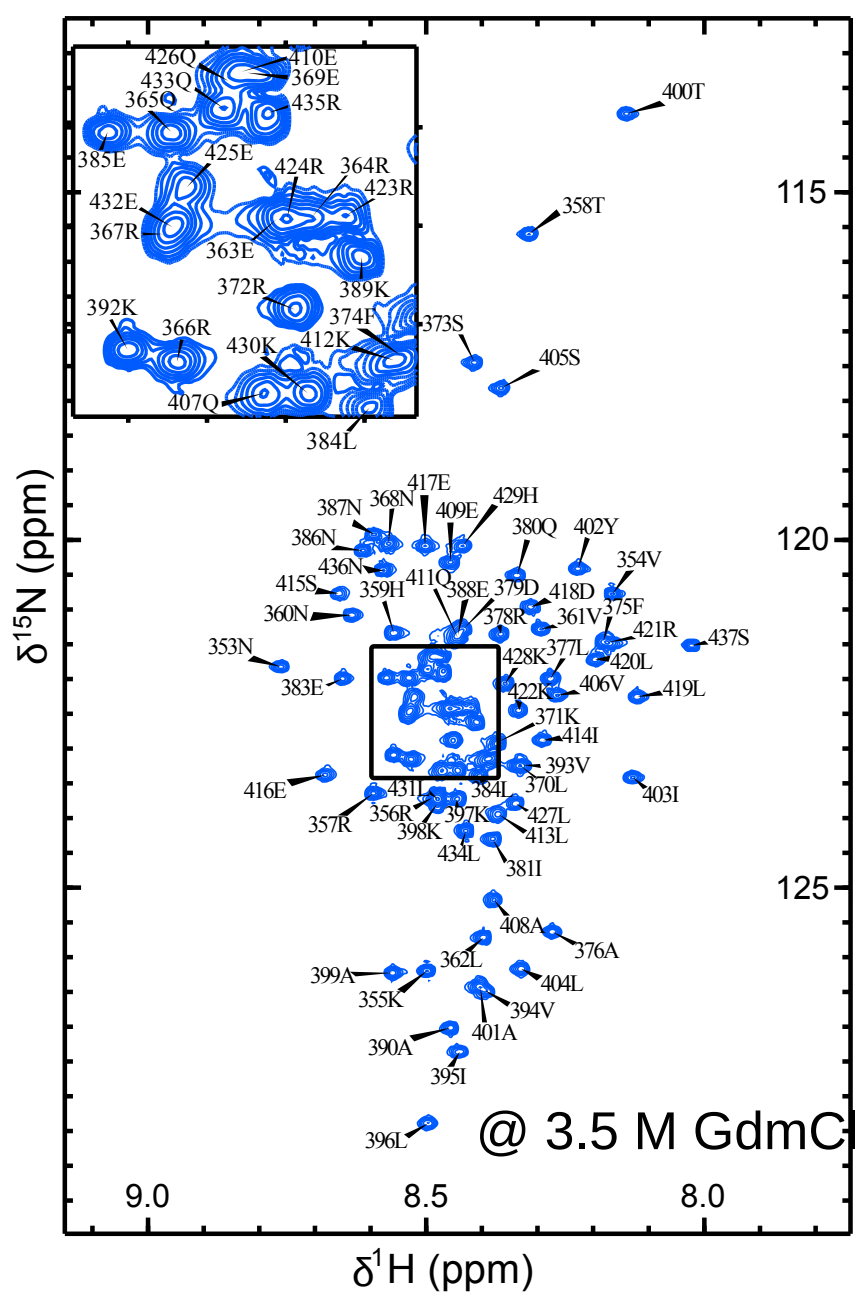
If you consider content in White Rose Research Online to be in breach of UK law, please notify us by emailing eprints@whiterose.ac.uk including the URL of the record and the reason for the withdrawal request.



eprints@whiterose.ac.uk
<https://eprints.whiterose.ac.uk/>



Chemical
denaturant
titration



Title:**Mapping hidden residual structure within the Myc
bHLH-LZ domain using chemical denaturant titration**

Authors: Stanislava Panova¹, Matthew J. Cliff¹, Pavel Macek^{2,3}, Martin Blackledge⁴, Malene Ringkjøbing Jensen⁴, J. Willem M. Nissink⁵, Kevin J. Embrey², Rick Davies², & Jonathan P. Waltho^{1,6,7*}

Author affiliations:

¹ Manchester Institute of Biotechnology, University of Manchester, Manchester, M1 7DN, UK.

² Discovery Sciences, IMED Biotech Unit, AstraZeneca, Alderley Park, SK10 4TG, UK.

³ NMR-Bio, Institut de Biologie Structurale, Grenoble Cedex 9, France

⁴ Univ. Grenoble Alpes, CNRS, CEA, IBS, F-38000 Grenoble, France

⁵ Oncology, IMED Biotech Unit, AstraZeneca, Cambridge, CB2 0AA, UK.

⁶ Molecular Biology and Biotechnology, University of Sheffield, Sheffield, S10 2TN, UK

⁷ Lead contact

*Correspondence: j.waltho@manchester.ac.uk

1
2
3 **Summary (150 words)**
4

5 4 Intrinsically disordered proteins (IDPs) underpin biological regulation and hence are highly
6
7
8 5 desirable drug-development targets. NMR is normally the tool of choice for studying the
9
10 6 conformational preferences of IDPs but the association of regions with residual structure into
11
12
13 7 partially collapsed states can lead to poor spectral quality. The bHLH-LZ domain of the
14
15 8 oncoprotein Myc is an archetypal example of such behaviour. To circumvent spectral
16
17 9 limitations, we apply chemical denaturant titration (CDT) NMR, which exploits the predictable
18
19
20 10 manner in which chemical denaturants disrupt residual structure and the rapid exchange
21
22 11 between conformers in IDP ensembles. The secondary structure propensities and tertiary
23
24
25 12 interactions of Myc are determined for all bHLH-LZ residues, including those with poor NMR
26
27 13 properties under native conditions. This reveals conformations that are not predictable using
28
29
30 14 existing crystal structures. The CDT-NMR method also maps sites perturbed by the prototype
31
32 15 Myc inhibitor, 10058-F4, to areas of residual structure.
33

34 16
35
36
37 17 **Keywords:** Intrinsically Disordered Proteins, Myc, Guanidinium Chloride, Molten globule,
38
39 18 Solution NMR, paramagnetic relaxation enhancement.
40
41

1 Introduction

2 Intrinsically disordered regions of proteins or entire intrinsically disordered proteins (IDPs) are
3 extremely prevalent in higher eukaryotes, and are involved in a wide range of biologically
4 important processes, such as extracellular communication, intracellular signalling, DNA
5 replication and transcription (Babu et al., 2011; Habchi et al., 2014; Oldfield and Dunker, 2014;
6 Wright and Dyson, 2015). The conformational ensemble defined as disordered does not
7 necessarily represent a purely random coil state, and different IDP sequences exhibit different
8 behaviours, ranging from rapidly-rearranging disordered coils, to more collapsed states with
9 long-range contacts and persistent secondary structure elements. These latter IDPs can be
10 classified as having molten globule -like behaviour, characterised by a loose core without the
11 precise packing of folded proteins (van der Lee et al., 2014). Molten globule -like behaviour is
12 observed in a range of states from native-like folds with dynamic interiors (e.g. apo-
13 myoglobin), to ensembles with low hydrodynamic radii but no persistent structure. IDPs that
14 display this behaviour are frequently involved in molecular recognition and some adopt
15 conventional globular structures when in complex with a binding partner. The basic-helix-loop-
16 helix-leucine zipper (bHLH-LZ) domain of the oncoprotein Myc is an archetypal example of
17 such behaviour.

18 Myc is an important transcription factor for cell growth, metabolism and apoptosis, and its
19 overexpression is associated with many cancers (Santarius et al., 2010). Transcriptional activity
20 of Myc requires hetero-dimerization with the protein Max. Both proteins have disordered
21 bHLH-LZ domains, which become ordered upon heterodimer formation, leading to the
22 recognition and binding of the E-box DNA sequence (Blackwood and Eisenman, 1991; Nair
23 and Burley, 2003; Prendergast et al., 1991). This makes small molecule inhibitors that disrupt
24 the Myc-Max interaction attractive candidates to be used as anticancer agents (Follis et al.,

1 2009; Metallo, 2010), but their development is limited by a lack of appropriate characterisation
2 of Myc in the IDP state adopted when isolated from Max.

3
4 3 Conventional structural biology techniques are not well-suited for IDPs, because any tertiary
5 structure is transient. NMR spectroscopy provides a number of informative measurements,
6 including chemical shifts, residual dipolar couplings and paramagnetic relaxation enhancement
7 (PRE) (Bhowmick et al., 2017; Jensen et al., 2014; Sormanni et al., 2017). PREs report on
8 interactions up to 30 Å, and on rarely populated states (<5%) (Baldwin and Kay, 2009; Clore,
9 2013; Salmon et al., 2010). However, IDPs present challenges to standard NMR techniques;
10 low structural complexity results in poor signal dispersion, although this is ameliorated by the
11 intense resonances observed for fully denatured proteins, and exposed amide groups are subject
12 to signal loss through solvent exchange, although this can sometimes be ameliorated using ¹³C-
13 detection (Bermel et al., 2012; Goradia et al., 2015; Wiedemann et al., 2015). IDPs that have
14 molten globule -like behaviour are more problematic, because the underlying conformational
15 exchange typically occurs on timescales that result in severely attenuated NMR resonances.
16 The signal attenuation is proposed to arise from averaging between many conformers with a
17 large range of barrier heights defined by a rough protein conformation energy landscape
18 (Milanesi et al., 2012).

19 Here, the structure propensity of the isolated bHLH-LZ domain from Myc has been extensively
20 characterised using chemical denaturant titration NMR (CDT-NMR). Under native-like
21 conditions, the molten globule -like behaviour of Myc results in residues of the leucine zipper
22 region producing no detectable resonances. We resolve this problem by shifting the solution
23 equilibrium towards a monomeric, less collapsed state (McParland et al., 2002; Reed et al.,
24 2006); titration with increasing guanidinium chloride (GdmCl) induces a cooperative transition
25 of Myc to a more disordered state. The GdmCl dependence is used to extrapolate chemical
26 shifts back to native conditions and to analyse the PREs of three singly MTSL-labelled cysteine

1 variants. The data reveal considerable helical structure under native conditions, especially in
2 part of the leucine zipper region. There is also significant tertiary contact between residues in
3 the helix 2-leucine zipper boundary region and those of helix 1 that is quite different to what is
4 observed in the Myc-Max crystal structure (Nair and Burley, 2003). The CDT-NMR approach
5 also allows the interaction with the prototype Myc inhibitor, 10058-F4, to be identified as
6 specifically affecting this tertiary contact in the molten globule -like state of Myc.

7 **Results**

8 **Assignment of bHLH-LZ domain NMR spectra.**

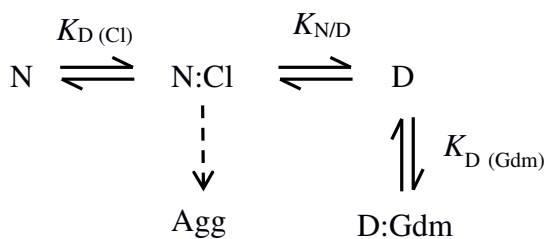
9 The ^{15}N - ^1H HSQC spectra of the bHLH-LZ domain of Myc (residues 352-437) in native-like
10 conditions (20 mM phosphate, 0.1 M NaCl, pH 7.4, 298K) shows only 46 out of 83 possible
11 cross-peaks (**Fig. 1a**). The detected peaks are broad, while retaining the poor dispersion
12 expected of a fully disordered protein. Therefore, residual order is slowing motion to a
13 timescale that causes the intensity of some resonances to be completely attenuated by NMR
14 relaxation. Changes in NaCl concentration, pH and acquisition temperature failed to increase
15 the number of detected peaks (described in Methods). In contrast, introduction of chemical
16 denaturant substantially improved the spectra. All 83 expected backbone amide signals are
17 observable at 0.6 M GdmCl and above, and all resonances have narrow linewidths (<14 Hz for
18 ^1H) at 3.2 M GdmCl (**Fig. 1b**).

19 Residue-specific assignment of all backbone amide resonances was completed at 3.2 M GdmCl
20 using conventional triple resonance experiments, and an additional (H)N(CA)NNH experiment
21 for regions where the C_α dispersion is poor. The $^1\text{H}_\text{N}$ and $^{15}\text{N}_\text{H}$ chemical shifts were observed to
22 change continuously in a titration from 3.2 to 0 M GdmCl, allowing the assignment to be
23 transferred to other GdmCl concentrations. HNCACB spectra were recorded at 2.4, 1.6 and 0
24 M of GdmCl to verify the assignment at these GdmCl concentrations. The resonances that are
25 missing in the absence of GdmCl correspond to the C-terminal residues of Myc (400-437), and

1 constitute part of the second helix (H2) and the whole leucine-zipper (LZ) region in the Myc-
2 Max crystal structure (secondary structure shown in **Fig. 2a**).

3 **Three categories of response to denaturant**

4 The responses of the NMR resonances to GdmCl were categorized into three distinct behaviour
5 types (**Fig. 2a & b**). For some residues (Blue category **Fig. 2a & b**), the largest chemical shift
6 changes occur at low GdmCl concentration (<0.6 M) where both $\delta^1\text{H}_\text{N}$ and $\delta^{15}\text{N}_\text{H}$ have the same
7 hyperbolic relationship with GdmCl concentration. These transitions correspond well with the
8 behaviour when GdmCl is replaced by NaCl in the titrations (**Fig. S1**). Hence, the effect is
9 independent of the cation present and therefore is ascribed to interaction with Cl^- ions. The
10 simplest model of a binding interaction is adequate to describe the data but the interaction with
11 Cl^- may not be a direct binding event, and may also involve formation of Myc homodimers
12 (Blackwood and Eisenman, 1991). For a second group of residues (Red category **Fig. 2a & b**),
13 the $\delta^1\text{H}_\text{N}$ and $\delta^{15}\text{N}_\text{H}$ changes have a sigmoidal dependence on GdmCl concentration with a mid-
14 point at ~1.2 M. There is no equivalent transition with NaCl and so the effect is ascribed to the
15 Gdm^+ ions and is indicative of a folding event with some cooperativity. A third group of
16 residues (Green category **Fig. 2a & b**) are subject to both effects and, in contrast to the other
17 categories, these ^1H - ^{15}N crosspeaks follow a significantly curved path as the denaturant
18 concentration changes. Additionally, all residues show a weak linear dependence on GdmCl
19 concentration, which persists at high denaturant concentrations (>2.5M). This likely reflects a
20 weak interaction between Gdm^+ and the protein backbone (Plaxco et al., 1997), analogous to
21 the well-established effect of urea (Huang et al., 2012; Meier et al., 2007). The total reaction
22 scheme for the interaction between Myc and GdmCl is described by *Scheme 1*:



Scheme 1

where N stands for native disordered state of Myc, D for denatured and N:Cl and D:Gdm indicate the bound forms. The dotted arrow represents a very slow precipitation of Myc in the presence of elevated Cl^- concentrations, which is countered by Gdm^+ ions.

The parameters defining the Cl^- interaction and the cooperative folding event were fitted globally to *Equation 1* using δ^1H_N and $\delta^{15}N_H$ values for a subset of residues with large chemical shift changes, and then fixed when fitting the chemical shift changes for all residues. All residues are fitted satisfactorily with global parameters for the underlying physical processes (examples in **Fig. 2b**). Fitting the chemical shift changes using the global parameters allows the extrapolation of the incomplete datasets to 0 M GdmCl, thereby providing estimates of δ^1H_N and $\delta^{15}N_H$ values where none could be determined experimentally. The accuracy of these estimates was determined to be 0.03 ppm for δ^1H_N and 0.3 ppm for $\delta^{15}N_H$ (see Methods). Using $\Delta\delta^1H_N$ and $\delta^{15}N_H$ values in the global fitting procedure rather than the standard chemical shift perturbation formula $((\Delta\delta^1H_N)^2 + (\Delta\delta^{15}N_H/6)^2)^{0.5}$ produced more consistent fit parameter values, particularly for residues in the green category (**Fig. 2b**), because the root - sum of squares function does not account for the direction of chemical shift changes.

The sequence distribution of the resulting chemical shift changes corresponding to each transition is shown in **Fig. S2**. The derived K_D value for the interaction with Cl^- (410 mM) is consistent with weak, non-specific binding, which is focussed at hotspots around the KRR sequence (residues 355-357) and around residue A390, which in the Myc-Max crystal structure correspond to the N-terminal basic H1 region and the turn region, respectively. The signal

1 attenuation observed at low denaturant concentration precluded analysis of the Cl⁻ interaction
2 for much of the C-terminal region. The best fit parameters for the cooperative folding transition
3 indicate weak stability (-6.2 kJ.mol⁻¹) and a low Gdm⁺ *m*-value of 2.8 (equivalent to 6.5
4 kJ.mol⁻¹.M⁻¹(Clarke and Waltho, 1997; Myers et al., 1995)) for the more folded species; values
5 typical of partially ordered states (Cliff et al., 2009; Reed et al., 2006; Scholtz et al., 2009). The
6 final two heptad repeats of the LZ (residues 426-436) in the Myc-Max crystal structure show
7 the largest chemical shift changes for this transition, and are in the region with large signal
8 attenuations in native-like conditions. The gradients of the weak linear dependence of chemical
9 shift on GdmCl concentration, visible at high denaturant concentrations, are also largest for the
10 C-terminal residues.

11 **α-Helical structure is populated at low denaturant concentrations**

12 The changes in chemical shift with denaturant suggest that the conformational distribution of
13 the polypeptide chain is changing. Whilst some of these changes can be ascribed to weak
14 interactions with Cl⁻ or Gdm⁺, the cooperative transition is consistent with structural changes
15 that alter the exposure of hydrophobic surface area (Scholtz et al., 2009). The backbone ¹H, ¹⁵N
16 and ¹³C chemical shifts were analysed to determine whether these changes corresponded to a
17 change in secondary structure propensity (SSP). Full data sets ($\delta^1\text{H}_\text{N}$, $\delta^{15}\text{N}_\text{H}$, $\delta^{13}\text{C}_\alpha$, $\delta^{13}\text{C}_\beta$) were
18 available at 1.6, 2.4 and 3.2 M GdmCl, with additional data at 0 M for residues 352-395. The
19 $\Delta\delta^{13}\text{C}$ values have a strong correlation with $\Delta\delta^{15}\text{N}_\text{H}$ values for the same residue (**Fig. S3**) and
20 so $\delta^{13}\text{C}_\alpha$ and $\delta^{13}\text{C}_\beta$ were extrapolated back to 0 M GdmCl using the fitted $\Delta\delta^{15}\text{N}_\text{H}$ values from
21 the analysis above, which allowed estimation of SSPs for residues 400-437. The accuracy of
22 the extrapolations was determined to be 0.23 ppm for both $\delta^{13}\text{C}_\alpha$ and $\delta^{13}\text{C}_\beta$ (see Methods).

23 Two helical clusters can be distinguished (residues 359-373 and 400-436), which dissolve upon
24 addition of GdmCl (**Fig. 3**). In particular, the region from residues 416-422 (SEEDLLR) is
25 predicted to be 90% helical in the absence of denaturant. These clusters are also helical in the

1 Myc-Max crystal structure. However, the reverse is not always true; for example the residues of
2 the first turn of H2 in the Myc-Max crystal structure (393-396, VVIL) have a significant strand
3 or PPII-helix propensity in isolated Myc at 0 M GdmCl. The chemical shifts for several
4 residues do not reach random coil values at 3.2 M GdmCl, with up to 30% helical content
5 remaining in the LZ region. It is notable that the region of greatest helix content determined
6 from $\delta^{13}\text{C}$ values does not co-locate to the region of greatest $\delta^{15}\text{N}_\text{H}$ perturbation by GdmCl
7 (**Fig. S2**), which lies between residue Q426 and the C-terminus.

8 **Paramagnetic relaxation enhancements detect a tertiary contact at low denaturant**

9 The secondary structure information present in chemical shifts is complemented by tertiary
10 contact information from paramagnetic relaxation enhancement (PRE) measurements. A
11 number of single cysteine variants were screened for optimal protein expression, and three were
12 prepared and labelled using the nitroxide spin-label MTSL, namely Q365C-SL, N386C-SL and
13 S405C-SL. The denaturant titration profiles for the derivatised variants are very similar to the
14 equivalent profiles for wild-type Myc (**Fig. S4**), with crosspeaks being readily assigned by
15 direct comparison of spectra. In the absence of denaturant, no data are available for residues
16 400-437 because of the signal attenuation described above. In order to gain tertiary contact
17 information from the line-broadened peaks, PREs were measured as a function of denaturant
18 concentration, and *Equation 2* was used to extrapolate PRE values for residues with attenuated
19 signals at 0 M GdmCl, using the parameters defined by the analysis of chemical shift changes
20 (Cliff et al., 2009) (see **Fig. 4** for example profiles).

21 For all three spin-labelled variants, there is a strong denaturant dependence for the measured
22 PREs. At 0 M GdmCl (**Fig. 5a**), the sequence distribution of the resulting intensity ratios
23 ($I_{\text{para}}/I_{\text{dia}}$) is broad. The Q365C-SL variant reports significant contacts throughout the 355-390
24 region, with lower effects up to residue Q407, but little contact with the C-terminal region. The
25 N386C-SL variant reports contacts throughout the same region, with the primary effect

1 occurring between residues Q365 and A399. In contrast, the S405C-SL variant reports contacts
2 over much more of the sequence, with the primary effects broadly centred around residue F375
3 and, to a lesser extent, around residue E425. Effects observed for residues before Q365 and
4 between E385 and A390 are lower, indicating there is a preferential contact between S405 and
5 the F375 region compared with the intervening residues. At 3.2 M GdmCl (**Fig. 5b**), the PREs
6 from each spin-labelled variant largely follow the behaviour expected for a fully disordered
7 protein, but with some low PREs (i.e. intensity ratios less than 2 standard deviations below that
8 expected for a random coil) at sequence distant positions. The Q365C-SL variant reports
9 contacts extending to K355 and Q407, while the N386C-SL variant reports contacts to the
10 region between residues Q365 and R378. The S405C-SL variant reports contacts to the region
11 between residues E363 and E385. Hence, the simplest model is that the observed PREs at this
12 GdmCl concentration reflect the rare population of species that resemble the native disordered
13 state.

14 Overall, the primary long-range contacts detected in the native disordered state are consistent
15 between the three spin-label variants and occur between regions around F375 and around T400,
16 and between around L370 and around E385. The former contact is close to an intramolecular
17 contact within Myc present in the Myc-Max crystal structure, where the C-terminus of H1
18 interacts with H2. In order to test how consistent the measured PREs are with this folded state
19 of Myc, values were calculated on the basis of an isolated Myc monomer from the crystal
20 structure conformation, and a modelled Myc homodimer (using Max as a template) (solid lines
21 in **Fig. 5a**). This established that the native disordered state of Myc is a much more dynamic
22 system as the PRE data are, in general, inconsistent with ordered, folded states; the calculated
23 profiles for folded Myc show significant peaks and troughs throughout the sequence (blue line
24 in **Fig 5a**). For the Q365-SL variant, the distribution of PREs is very different to the calculated
25 values, particularly around residues A390 and S415, indicating substantial non-native character.

1 However, for the S405-SL variant, the distribution, though not the size, of PREs more closely
2 resembles the calculated values from the folded structures.

3 The NMR properties exhibited by the native disordered state of Myc may reflect transient
4 intramolecular or intermolecular interactions, or a combination of both. Consistent with a self-
5 association component, the broadening of resonances for LZ residues showed a small
6 dependence on protein concentration below 1.2 M GdmCl. Consequently, PREs were measured
7 as a function of protein concentration to determine the extent to which intermolecular contacts
8 contributed to the native disordered state. Changes in intensity ratios of less than 10% were
9 observed upon 10-fold dilution (**Fig. S5**). In addition, MTSL-derivatised ^{14}N Myc had a
10 negligible PRE effect on the NMR spectrum of underderivatised ^{15}N -labelled Myc, at the lowest
11 GdmCl concentration where all peaks were visible. (**Fig. S6**). Therefore, the protein
12 concentration dependence of signal intensities of LZ residues is ascribed to viscosity or other
13 solvent effects rather than self-association, and the dominant relaxation enhancements and
14 chemical shift changes result from intramolecular contacts.

15 **The structure of the bHLH-LZ domain is compact and disordered.**

16 In order to visualise the properties of an ensemble that is consistent with the data, and to
17 allow calculation of macroscopic properties like the radius of gyration (R_g), the experimental
18 PREs and chemical shifts were used as input into Flexible Meccano/ASTEROIDS calculations
19 (Ozenne et al., 2012; Salmon et al., 2010). The extensive degrees of freedom available to IDPs
20 vastly outweigh the sparse experimental constraints, so the resulting ensemble does not reliably
21 predict chemical shift and PRE data other than those used as input. An initial pool of 10000
22 conformers was calculated based on the extrapolated chemical shift values ($^{13}\text{C}_\alpha$, $^{13}\text{C}_\beta$, $^1\text{H}_\text{N}$, ^1N)
23 at 0 M GdmCl. Five ensembles of 200 conformers that satisfied both the chemical shift and
24 PRE data were then selected from the initial pool using ASTEROIDS, and combined into a
25 final ensemble.

1 The calculated values for the final ensemble correspond well to the experimental ones (**Fig.**
2 **S7**). Per-residue secondary structure propensities in the final ensemble (example Ramachandran
3 plots are shown in **Fig. 6a**) are consistent with the SSP predictions above (**Fig. 3**) and show that
4 two main regions of ψ , ϕ space dominate, α -helical and PPII (**Fig. 6b**). The β -strand region is
5 less populated, with just one residue, I381, predominantly (~60%) in this conformation. The
6 416-421 region shows almost 100% α -helicity, in close agreement SSP predictions based solely
7 on chemical shift.

8 The contact map and the distribution of R_g values calculated from the final ensembles (**Fig. 6c**
9 **& d**) illustrate that residues in the 360-380 region are closer to residues in the 400-410 region
10 than would be expected for a random coil ensemble, consistent with the experimental PRE data
11 (**Fig. 5**). Correspondingly, the R_g distribution peaks at 23 Å, which is 5 Å smaller than in the
12 distribution for the initial pool. The compaction is not as large as for the formation of the Myc-
13 Max crystal structure ($R_g = 18$ Å), and while there are some preferential conformations, the
14 ensemble is largely disordered. Representative protein conformations (**Fig. 7**) illustrate the
15 distribution of helical segments, and the absence of common tertiary structure.

16 **Structure in relation to ligand binding.**

17 A number of molecules that specifically interact with Myc have been reported (Metallo, 2010),
18 but thus far their mode of interaction has been difficult to define (Follis et al., 2008;
19 Hammoudeh et al., 2009; Harvey et al., 2012; Heller et al., 2017). Hence, we investigated
20 whether the CDT-NMR approach could help elucidate the interactions of a molten globule -like
21 IDP with a ligand. The archetypal Myc-targeting molecule, 10058-F4, has an antiproliferative
22 action in cell cultures that is consistent with interrupting the Myc-Max interaction (Yin et al.,
23 2003). Initial NMR studies under native conditions showed some signs of interaction between
24 the measurable resonances of Myc and 10058-F4, but these effects were small, meaning that
25 other solvent effects such as protein and DMSO concentration variations could not be

1 discounted. Therefore, the experiments were repeated at Gdm⁺ concentrations where there is
2 significant population of the molten globule -like state, but the population of the denatured state
3 produces more favourable NMR relaxation behaviour and therefore higher spectral quality.

4 For this system, the optimal conditions were 0.5 M GdmCl, where the equilibrium
5 position is 80% molten globule -like and 20% denatured, according to the best fit parameters
6 for the data in **Fig. 2b**. Under these conditions, 10058-F4 induces significant attenuation of ¹H-
7 ¹⁵N HSQC crosspeaks, although only minor chemical shift changes (**Fig. 8a**), consistent with
8 slow intermediate exchange. However, whilst the distribution of affected residues is quite broad
9 (**Fig. 8b**), it has a pattern that resembles the PRE profiles (**Fig. 5**), rather than one that
10 resembles the transition between the denatured and molten globule -like states. The greatest
11 loss of intensity is at a region around T400 (shown as isolated orange peaks in **Fig. 8a**), with a
12 weaker effect at residues 360-380. In contrast, residues from K420 onwards are relatively
13 unaffected. This is consistent with the interaction between 10058-F4 and Myc specifically
14 stabilising the previously identified weak tertiary interaction between the 360-380 and 400-410
15 regions (**Fig. 5**), rather than stabilising all regions with molten globule -like behaviour. The
16 concentration of 10058-F4 is low (1 mM), so the most probable mechanism is by a specific
17 direct interaction with Myc rather than a solvent effect. The region showing greatest intensity
18 loss corresponds to one that has complete signal attenuation under native conditions (**Fig. 1a**),
19 making it difficult to identify using standard NMR approaches. No interaction is apparent at
20 GdmCl concentrations above 0.8 M, due to the low population of residual structure, indicating
21 that the optimal Gdm⁺ concentration to investigate ligand binding in different systems will
22 firstly need to be established using CDT-NMR.

23 Discussion

24 Previous work on chemically denatured proteins demonstrated that they rapidly
25 interconvert between denatured states with random coil behaviour and more compact, molten

1 globule -like states, with the population of the more compact forms increasing as conditions
2 become more native-like (Candotti et al., 2013; Cliff et al., 2009; Schulman et al., 1997). NMR
3 measurements reflect the ensemble average behaviour, and measurements under a range of
4 conditions can allow the contribution of sub-populations to be deconvolved. Molten globule -
5 like states frequently have very poor NMR characteristics, with low resonance dispersion and
6 fast relaxation (leading to broad resonances and signal attenuation), and so the chemical
7 denaturant titration (CDT) method allows the determination of otherwise hidden behaviour.
8 The data here show that the Myc bHLH-LZ domain is an IDP with such molten globule -like
9 behaviour. The per residue folding parameters associated with the regions of Myc with high
10 structure propensity are similar enough that chemical shift data for all residues can be fitted
11 with common values, but the parameters do not necessarily describe a transition between states
12 that is concomitant across the molecule. They are more likely to reflect that individual local
13 clusters have similar hydrophobic burial and stability, but mostly form independently of each
14 other.

15 Previous NMR studies of Myc behaviour have used viral isoforms (v-Myc (Fieber et al.,
16 2001)), variants with some or all of the bHLH-LZ region missing (B-Myc (Burton et al.,
17 2006)), or short peptides derived from the Myc sequence (Hammoudeh et al., 2009; Lavigne et
18 al., 1998). Such studies can be argued not to fully represent the behaviour of the wild-type
19 protein in conditions most relevant to the cellular environment, and to small molecule based
20 intervention in disease states. In this study, significant helical propensity is seen throughout the
21 Myc sequence, and matches well the helical regions identified in v-Myc (Fieber et al., 2001)
22 and short peptides. Furthermore, the method has also allowed PRE measurements to determine
23 longer range interactions and give a fuller description of the structure propensity of the domain.
24 The ensemble calculation suggests that no particular conformation dominates, but the average
25 R_g is considerably smaller than for a random coil. The tertiary contacts in the ensemble are

1 consistent with the results of a recent molecular dynamics study, which suggest that Myc has a
2 tendency to form a hairpin-like conformation (Liu et al., 2017).

3 The structural elements defined for Myc in the absence of denaturant are potentially
4 functionally important. The region with the greatest helical content (>90% helical; residues
5 416-422, **Fig. 3**) corresponds to the position within the leucine zipper that is important in
6 ensuring specificity for the interaction with Max, and mutation of residues E417, R423 and
7 R424 results in significant homodimerisation (Soucek et al., 1998). The long-range tertiary
8 contact defined by the PREs (between the 360-380 and 400-410 regions) coincides with the
9 phosphorylation sites S373 and T400 (Macek et al., 2018), suggesting that phosphorylation
10 perturbs this conformational ensemble, leading to its role in the mechanism of gene regulation.
11 In addition, mutation of R367 is sufficient to allow homodimerisation (Beaulieu et al., 2012),
12 an effect that is ascribed to electrostatic repulsion, but might be caused by the stabilisation of
13 non-native contacts. Furthermore, the regions of tertiary contacts coincide with the regions that
14 are affected by the small molecule inhibitor, 10058-F4, suggesting that a similar regulatory
15 effect can be induced by pharmaceuticals, and holds hope for the design of further drug
16 candidate molecules.

17 Non-random coil behaviour in disordered protein chains is well-established, both for
18 conventionally folded proteins (N-PGK (Cliff et al., 2009), Drk-SH 3 (Marsh et al., 2007),
19 Staph Nuclease (Zhang et al., 1997)), and for IDPs. For example, our results broadly resemble
20 those obtained with spin-labelled variants of α -synuclein (Bertoncini et al., 2005; Dedmon et
21 al., 2005), which in combination with residual dipolar couplings (RDCs), defined tertiary
22 interactions to be present in the absence of denaturant, and that contribute even at 8 M Urea.
23 The interactions are between the C-terminus and the aggregation prone NAC region of α -
24 synuclein. Studies with Tau show it to have both compact and extended regions (Schwalbe et
25 al., 2014), whereas the contact map for Myc shows higher level of compactness for most

1 regions of the construct. On the basis of these studies with Tau and α -synuclein, a link was
2 proposed between polyproline II propensity and aggregation prone precursors for pathogenic β -
3 strand formation, but while there are polyproline II favoured regions in Myc, which coincide
4 with the loop in Myc-Max crystal structure, the NMR data show they are not prone to
5 aggregation.

6 In conclusion, chemical denaturant titration NMR (CDT-NMR) has allowed us to
7 explore fully the conformational ensemble of a wild-type protein domain containing all the
8 elements required to interact with its binding partners, Max and DNA, despite many resonances
9 being broadened beyond detection in the absence of denaturant, and others having little or no
10 intensity in triple-resonance spectra. The application of the CDT method extends from previous
11 Myc studies by allowing the delineation of native behaviour from that of the chemically
12 denatured state. The utility of the CDT-NMR method for regions that have poor spectral
13 properties in the absence of denaturant has allowed the behaviour of the leucine zipper region
14 to be determined, which has not been possible using previous methods. The signals that are
15 most attenuated by conformational exchange are inherently those with the strongest structure
16 propensity. It follows from the conventional structure-function paradigm that such regions are
17 most likely to be functionally significant (as here, the most structured region defines Myc-Max
18 specificity) and, potentially, the most druggable. Even in fuzzy complexes, where the structure
19 function paradigm does not apply so rigourously, specificity is likely to be defined by small
20 clusters of transient structure. Having defined the denaturant dependence of structured regions,
21 a system can be poised at an equilibrium position where the contribution from more compact
22 conformers is significant, but not sufficient to attenuate the NMR signals deleteriously. This
23 approach can be used, for example, to delineate interactions with inhibitors, making IDPs with
24 molten globule -like behaviour amenable to hitherto prohibited screening of lead drug

1 compounds. The method should also be compatible with other NMR measurements such as
2 RDCs, and the identification of protein-protein interactions.

3 **Acknowledgements:**

4 SP PhD studentship was funded jointly by Bruker and a President's Doctoral Scholar Award of
5 the University of Manchester, PM was an AZ funded post-doctoral researcher. All data
6 recorded at Manchester Biomolecular NMR facility.

7 **Declaration of Interests**

8 JWMN, KJE and RD are employees of the AstraZeneca and may have stock/stock options in
9 AstraZeneca PLC.

10 **Author Contributions**

11 S.P. produced and purified the protein, performed NMR experiments, analysed the data, and
12 wrote the paper. M.J.C. designed experiments, analysed the data and wrote the paper. P.M.
13 designed protein constructs, carried out NMR experiments and analysed data. M.R.J. and M.B.
14 performed the structural ensemble selections using ASTEROIDS. J.W.M.N., K.J.E. and R.D.
15 designed and coordinated experiments. J.P.W. supervised the project. All authors discussed
16 results and commented on the manuscript.

17 **Figure Legends**

18 **Figure 1:** (a) ^1H - ^{15}N HSQC spectrum of Myc bHLH-LZ domain under the standard buffer
19 conditions and 0 M GdmCl, (b) ^1H - ^{15}N HSQC spectrum of Myc bHLH-LZ domain under the
20 standard buffer conditions with addition of GdmCl to 3.2 M. Amide cross peaks are labelled
21 with the residue number and single letter code for their assigned amino acid. No peaks are
22 visible in spectrum (a) for residues 400-437. Inset in (b) shows the crowded region marked
23 with a box in the centre of the spectrum.

24 **Figure 2.** (a) Primary structure of Myc bHLH-LZ domain with residues colour coded
25 according to category of behaviour, mostly hyperbolic (blue), mostly sigmoidal (red) and

1 showing both transitions (green), with the secondary structure boundaries taken from the Myc-
2 Max crystal structure 1nkp (B: basic helix, H1: helix 1, H2, helix 2, LZ; leucine zipper heptad
3 repeats). Circle radii reflect the uncertainty in the chemical shift measurements (0.005 ppm for
4 $\delta^1\text{H}_\text{N}$ and 0.02 ppm for $\delta^{15}\text{N}_\text{H}$). (b) Titration behaviour of amide crosspeaks for a selection of
5 residues. Top row shows positional changes in ^1H - ^{15}N HSQC spectra with the axes origin
6 indicating the starting chemical shift (lowest concentration of GdmCl giving a visible peak).
7 Middle row and bottom row show $\delta^1\text{H}_\text{N}$ and $\delta^{15}\text{N}_\text{H}$ (respectively) behaviour as a function of
8 GdmCl concentration. Solid lines show behaviour expected from the best fit parameters
9 generated by a global fit to *Equation 1* (see **Methods**), where chemical shift related parameters
10 are varied for each residue, but underlying physical constants reflect the whole protein. The
11 best fit global parameters are $K_{\text{N/D}} = 14 \pm 3$ (-6.2 ± 0.4 kJ.mol $^{-1}$), $m = -2.8 \pm 0.2$ (6.5 ± 0.4
12 kJ.mol $^{-1}$.M $^{-1}$), $K_{\text{D (Cl)}} = 410 \pm 40$ mM (14 kJ.mol $^{-1}$). The mean χ^2 was 12.9 with 24 degrees of
13 freedom.

14 **Figure 3:** Secondary structure prediction from SSP on the basis of $^{13}\text{C}_\alpha$ and $^{13}\text{C}_\beta$ chemical
15 shifts, at the labelled denaturant concentrations. Positive values indicate helix and negative
16 values indicate β -strand or PPII helix. Filled bars show predictions based on measured
17 chemical shifts, whereas predicted values for residues lost through signal broadening are shown
18 as open bars.

19 **Figure 4:** Denaturant dependence of PREs for example residues, showing best fit relationship
20 for *Equation 2* as solid lines. Crosspeak intensity ratios between paramagnetic and diamagnetic
21 samples are shown as circles, with the radii showing the calculated errors.

22 **Figure 5:** Sequence distribution of PREs ($I_{\text{para}}/I_{\text{dia}}$) at 0 M (a) and 3.2 M GdmCl (b), for each
23 spin-labelled variant. For residues that experience significant line-broadening (400-417), values
24 at 0 M GdmCl were based on the fits of denaturation profiles to *Equation 2*. In a, the solid lines
25 show the behaviour expected for the Myc-Max crystal structure monomer (black) and a

1 modelled homodimer (blue). In **b**, the red solid line shows the behaviour expected for a self-
2 excluding random coil with the sequence specific secondary structure propensity (an ensemble
3 generated by flexible mecano/ASTEROIDS).

4 **Figure 6:** Structural parameters for the ensemble selected by ASTEROIDS **(a)** Ramachandran
5 plots showing the amino acid conformational potentials for representative residues V354, L377,
6 K398 and L420 in the ensemble. **(b)** Populations of residues in the ensemble with dihedral
7 angles in particular regions of Ramachandran space: α -helix (green), PPII (dark-blue), β -strand
8 (red), with the PPII and \square regions being summed and defined as negative. The number of
9 conformers populating left-handed helix was negligibly small for all residues (<3%). Definition
10 of regions of Ramachandran space was done as described before (Ozenne et al., 2012). **(c)**
11 Distribution of radius of gyration (R_g) for the random coil (red) and the final PRE, chemical
12 shift-based ensemble (blue). R_g for the random coil state is 29 Å and decreases to 28 Å when
13 the chemical shifts are included in calculations. Inclusion of PRE data reduces this to 23 Å, a
14 compaction of 82%. The compaction expected from the Myc-Max crystal structure is 58%. **(d)**
15 Final contact map showing Myc long-range contacts derived using chemical shift and PRE
16 data. Heat-map represented in terms of log-ratio of the distance between residues in the selected
17 and chemical shift -based pool $\Delta_{ij} = \log(\langle d_{ij} \rangle / \langle d_{ij,ref} \rangle)$. Colours range from red (-0.4, regions
18 in closer contact than pool (see Methods)) to blue (0.0) to violet (0.2, regions farther apart than
19 pool).

20 **Figure 7.** Representative structures from the final ensemble selected by ASTEROIDS: a)
21 lowest R_g conformer, b) most frequently selected conformer c) closest to mean R_g conformer d)
22 mode R_g conformer. Structures are represented as a ribbon coloured blue to red, N- to C-
23 termini. Consistent helical region is in orange region.

24 **Figure 8:** Ligand binding at 0.5 M GdmCl. **(a)** HSQC spectra of 100 μ M Myc recorded at 0.5
25 M GdmCl and 5% DMSO-d₆, in the presence (dark blue) and absence (orange) of 1 mM

1 10058-F4. (b). Ratio of peak height for assigned resonances in the two spectra, showing regions
2 of Myc affected by the compound

3 4 **STAR Methods**

5 **CONTACT FOR REAGENT AND RESOURCE SHARING**

6 Further information and requests for resources and reagents should be directed to and will be
7 fulfilled by the Lead Contact, Jonathan Waltho (j.waltho@manchester.ac.uk).

8 **EXPERIMENTAL MODEL AND SUBJECT DETAILS**

9 Experimental model is recombinant, human Myc protein (RRID:SCR_008608) C-terminal
10 domain (bHLH-LZ) residues 351-437. It was expressed in *E coli* BL21(DE3) Gold from a pET
11 -derived vector with an N-terminal HisTag, which was removed by proteolysis during
12 purification. Standard conditions were defined as 20 mM phosphate buffer, pH=6.5, T=278 K,
13 with protein concentration 5mg/ml (410 μ M).

14 Four single cysteine mutants were prepared for site-specific electron spin-labelling; Q365C,
15 N386, S405C and Q411C.

16 **METHOD DETAILS**

17 The bHLH-LZ domain of Myc (residues 351-437) and the cysteine point-mutants were
18 expressed from a pET derived vector in *E. Coli* BL21 (DE3) Gold cell lines (Agilent
19 Technologies) at 37 °C (310 K) in M9 minimal medium supplemented with 2 g/L of ¹³C
20 glucose (or 4 g/L of ¹²C glucose) and 1 g/L ¹⁵N ammonium chloride (Sigma-Aldrich) as the
21 only carbon and nitrogen sources. Protein expression was induced by addition of 0.1 mM IPTG
22 to bacterial cultures at OD₆₀₀=0.9, which were harvested 4 h after induction and frozen at -80
23 °C. Cell pellets were resuspended in 20 mM phosphate buffer with 8 M urea and protease
24 inhibitor tablet “Complete” (Roche), sonicated and centrifuged for 30 min at 40000 g.
25 Supernatant was loaded on a Talon Co²⁺ affinity column, equilibrated with 3 M GdmCl, 20 mM
26 phosphate, 0.1 M NaCl, pH=7.4, washed by 2.5 mM imidazole and Myc was eluted by addition

1 of 125 mM imidazole. The His-tag was cleaved off by TEV protease and the resulting His-tag
2 peptides were removed by further Co^{2+} -affinity chromatography. The purity and identity of the
3 proteins were validated by electrospray ionization mass spectrometry (ESI-MS) and SDS-
4 PAGE.

5 Paramagnetic labelling of Myc was achieved by incubating Myc cysteine mutants with MTSL
6 (S-(1-oxyl-2,2,5,5-tetramethyl-2,5-dihydro-1H-pyrrol-3-yl)methyl methanesulfonylthioate;
7 Toronto Research Chemicals, Canada) in the presence of 3 M GdmCl and 1 mM DTT at RT in
8 the dark for 8 h. MTSL was present in 5:1 excess over the total thiol concentration. Reaction
9 completeness was confirmed by mass-spectrometry to be more than 95%. Samples were buffer
10 exchanged in 20 mM phosphate, 1 mM EDTA, pH 6.5.

11 Buffer conditions were screened and optimized to provide best spectral dispersion, highest
12 signal intensity and least visible aggregation for Myc samples. The buffer screen covered pHs
13 from 5 to 7.5 and NaCl concentrations up to 1.2 M, and used either phosphate or Bis-Tris to
14 control pH. The effect of temperature was also studied. Standard conditions were defined as 20
15 mM phosphate buffer, pH=6.5, T=278 K, with protein concentration 5mg/ml (410 μM).

16 All samples for NMR spectroscopy were prepared in 20 mM phosphate buffer, pH=6.5 and
17 varying concentration of GdmCl with addition of 10% D_2O and 1 mM TSP (Trimethylsilyl
18 propanoic acid). Except where stated, spectra were recorded at 278 K on a Bruker AVANCE III
19 800 MHz spectrometer equipped with a TCI cryoprobe (^1H - $^{13}\text{C}/^{15}\text{N}$ with z-gradients) in 3mm
20 tubes. Gradient selective, sensitivity-enhanced HSQC spectra had a spectral width of 20 ppm
21 (1622 Hz) and apparent acquisition time of 60 ms for the indirect dimension. Spectra were
22 processed using Topspin 3.2 software (Bruker Corp).

23 Protein backbone resonance assignment experiments were recorded for Myc at 3.2 M GdmCl,
24 comprising two-dimensional ^{15}N - ^1H HSQC and triple resonance experiments (H)N(CA)NNH,
25 HNCACB, HNCA, HNC(O), HN(CO)CA and HN(CO)CACB spectra. All spectra were collected

1 using Echo/Antiecho-TPPI gradient selection, which was efficient at suppressing signals from
2 GdmCl and other buffer components. Non-uniform sampling (NUS) was used to optimize
3 resolution of the indirect dimensions in the available experiment time. NUS acquired data were
4 process using MDD algorithm within Topspin. Spectra were visualised and analysed using
5 CCPN Analysis 2.3.

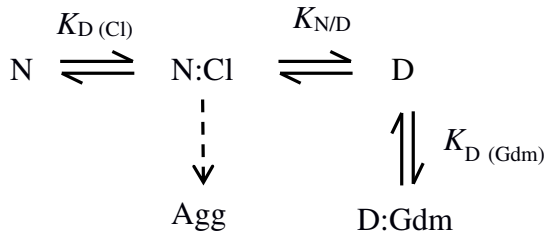
6 Two-dimensional ^1H - ^{15}N HSQC spectra were collected at a range of GdmCl concentrations
7 (from 0 to 3.2 M with 0.2 M step). In order to confirm validity of the resonance assignment
8 transfer between denaturant concentrations HNCACB spectra were collected for 2.4, 1.6 and 0
9 M GdmCl. This led to unambiguous assignment of Myc at native-like conditions even for very
10 low intensity peaks. In addition, a sodium chloride titration of Myc between 0 and 1.2 M (with
11 0.2 M step) was collected. To characterize the Myc self-association and aggregation, protein
12 concentrations (0, 0.025, 0.05, 0.1, 0.2, 0.4, 0.8 mM) were varied and ^1H - ^{15}N HSQC spectra
13 recorded, repeated at 0, 0.6, 1 and 2 M GdmCl.

14 Paramagnetic relaxation enhancement (PRE) data were collected for diamagnetic and
15 paramagnetic samples at a range of GdmCl concentrations (0 to 3.2 M with 0.3 M step).
16 Diamagnetic sample was obtained by addition of a 5-fold excess of sodium L-ascorbate to the
17 spin-labelled protein sample. Relaxation delays for ^{15}N - ^1H HSQC were 2 s, which was
18 sufficient to allow 90% signal recovery between transients.

19 QUANTIFICATION AND STATISTICAL ANALYSIS

20 Data were processed in Topspin 3.2 and quantified in CCPN Analysis 2.3. Data fitting
21 was by Levenberg-Marquadt non-linear least squares optimisation using in-house routines
22 interfacing with Numerical Python.

23 Chemical shifts were analysed as follows: the total reaction scheme for the interaction
24 between Myc and GdmCl can be described by the Scheme 1:



Scheme 1

where N stands for native disordered state of Myc, D for denatured and N:Cl and D:Gdm indicate the bound forms. The dotted arrow represents a very slow precipitation of Myc in the presence of elevated Cl^- concentrations, which is countered by Gdm^+ ions. Because the aggregation process is slow and irreversible, it doesn't contribute to chemical shifts. In addition, the dissociation constant for Gdm^+ binding to the unfolded state is so high (>4M) that the effect can be approximated by a linear function. Thus, the chemical shift data can be analysed according to the following simplified scheme:



$K_{D(Cl)}$ is the binding constant for chloride and $K_{N/D}$ is equilibrium constant between the denatured and the native disordered states. Proton chemical shift perturbation dependence by GdmCl was fitted to equation:

$$\delta H_i = \delta H_0 + \frac{\frac{[GdmCl]}{K_D} * (\Delta\delta H_{Cl} + (\Delta\delta H_{Gdm} + slope_H * [GdmCl]) * K)}{1 + \frac{[GdmCl]}{K_D} * (1 + K)} \text{ with } K = K_0 * e^{-m * [GdmCl]}$$

Equation 1

δH_0 is the initial value of the proton chemical shift difference for residues, $\Delta\delta H_{Cl}$ is the maximum chemical shift perturbation of the proton chemical shift by chloride and $\Delta\delta H_{Gdm}$ is the maximum effect of Gdm. K_0 is the value of K at 0 M GdmCl, m is the denaturant concentration dependence of the free energies. ^{15}N chemical shifts were fitted to the same equation. Initial fitting was to a subset of residues with clearly defined behaviour, fitting a K_D , K_0 and m as global parameters, and chemical shifts on a per residue basis. Subsequently, the values of K_D , K_0 and m were fixed in fits of all residues. No significant difference between the

1 fit-lines and the data points resulted. The efficacy of using the global parameters to allow
2 extrapolation to zero denaturant for residues with significant signal attenuation under such
3 conditions was tested by omitting data points below 0.6 M GdmCl for complete data sets and
4 repeating the fitting procedure. The RMS deviation between the fitted values and the recorded
5 chemical shifts was 0.03 ppm for δH and 0.3 ppm for δN . These uncertainties were propagated
6 into the estimates of ^{13}C chemical shifts.

7 $^{13}\text{C}_\alpha$ and $^{15}\text{N}_\text{H}$ chemical shifts changes for each residue were found to correlate, and so the
8 maximum ^{15}N shift defined by data fitting was used to calculate the $^{13}\text{C}_\alpha$ shifts at 0 M GdmCl
9 used for SSP. For residues with complete datasets, omitting the 0 M GdmCl point and repeating
10 the process gives a RMS difference from the recorded value of 0.37 ppm for C_α (0.23 after
11 excluding outliers H359 and F375) and similarly 0.75 ppm for C_β (0.23 after excluding the
12 same outliers). Neither of these outlier residues are in regions with strong secondary structure
13 propensity.

14 PRE effects were calculated from the intensity ratio of HSQC peaks between
15 paramagnetic and diamagnetic samples for each residue, and fitted to the following equation
16 (Cliff et al., 2009).

$$\frac{I_{ox}}{I_{red}} = \frac{R'_2}{R'_2 + R'_P} e^{-(R'_P \cdot t)} \text{ where } R'_x = \frac{R_x^D + R_x^N * K}{(1+K)} \text{ with } K = K_0 * e^{-m \cdot [\text{GdmCl}]} \quad \text{Equation 2}$$

17 The exchange between conformers is fast relative to the chemical shift timescale, and
18 therefore assumed to be fast on the ^1H -e relaxation timescale, and therefore the apparent
19 transverse relaxation rate in diamagnetic samples (R'_2) and the additional paramagnetic
20 relaxation rate (R'_P) are population weighted averages between the rates in the native, denatured
21 state (N) populated at 0 M GdmCl, and the denatured state (D) populated at high GdmCl
22 concentrations. The time t is the amount of time protons are transverse in the HSQC pulse

1 sequence, amounting to 10.6 ms. R_2^D was fixed at 7 Hz ($\times 2\pi$) and residue specific R_2^N values
2 were estimated from the guanidinium dependence of the intensities in the diamagnetic sample.
3 These needed correcting for the change in sensitivity of the probe with Cl^- concentration,
4 which is proportional to the change in proton pulse-length (p_D/p_{0M}).

$$I_{red,D} = I_{red,0M} \times \frac{p_D}{p_{0M}} \times \frac{R_2^I e^{-(R_2^I - R_2^U).t}}{R_2^U} \quad \text{Equation 3}$$

6 with R_2^I calculated as in Equation 2.

7 Ensemble calculation

8 An original ensemble created by *flexible meccano* (Ozenne et al., 2012; Salmon et al.,
9 2010) comprised 10,000 structures with the phi/psi angles corresponding to random coils. 50
10 random ensembles with 200 structures each were created and χ^2 values were calculated for each
11 ensemble. Then using ASTEROIDS (Salmon et al., 2010) genetic algorithm 5 ensembles with
12 200 structures each were selected on the basis of the best fit to the experimental chemical shift
13 data. SPARTA (Shen and Bax, 2007) was used for prediction of chemical shifts. From these
14 structures, 1000 phi/psi angles were extracted for each residue, which were used as a library to
15 build 8500 structures for the next iteration. Next iteration started with 8500 structures from the
16 previous calculation and 1500 structures created from the random coil library. This process was
17 repeated 5 times to avoid being trapped in local minima.

18 These final 10000 structures were used as a starting pool to fit the PRE and chemical
19 shift data simultaneously. ASTEROIDS was used to produce equivalent ensembles containing
20 100 structures (5000 evolution steps were used in the genetic algorithm). PREs were calculated
21 from ^1H R_2 values estimated from the ^1H -e $^-$ distance in each conformation, the INEPT delay,
22 the conformational sampling of the spin label relative to the backbone and the estimated
23 correlation time of the dipole interaction (5ns), as described elsewhere. (Salmon et al., 2010)

1 Long-range order was assessed in the final ensembles by calculating distance values
 2 normalized against the average distance values calculated for the chemical shift (CS) based
 3 ensemble:

$$\Delta_{ij} = \log \left(\frac{d_{ij}}{d_{ij}^0} \right)$$

4 where d_{ij} is the distance between residues i and j in the final (CS-PRE) calculated ensemble
 5 and d_{ij}^0 is distance between residues i and j for the CS calculated ensemble. These values were
 6 used to plot contact map.

9 DATA AND SOFTWARE AVAILABILITY

10 NMR chemical shifts have been deposited with the BioMagResBank with accession
 11 codes 27701, 27702, 27703 and 27704.

13 KEY RESOURCES TABLE

REAGENT or RESOURCE	SOURCE	IDENTIFIER
Bacterial and Virus Strains		
BL21 (DE3) Gold <i>E. coli</i> .	Agilent technologies	CAT# 230132
Chemicals, Peptides, and Recombinant Proteins		
Human Myc protein (RRID:SCR_008608) C-terminal domain (bHLH-LZ) residues 351-437	In-house	
¹³ C glucose	Sigma Aldrich	CAT# 389374
¹⁵ N ammonium chloride	Sigma Aldrich	CAT# 299251
Guanidinium Chloride	Sigma Aldrich	CAT#G4505
TEV protease	In-house	
Talon Co2+ affinity column	Sigma Aldrich	CAT#GE28-9575-02
Complete Protease inhibitors	Roche	CAT# 11697498001
MTSL (1-Oxyl-2,2,5,5-tetramethyl- β -pyrroline-3-methyl) Methanethiosulfonate	Toronto Research Chemicals	CAT#O875000

Deposited Data		
Backbone 1H, 13C, and 15N Chemical Shift Assignments for the Myc bHLH-LZ domain in presence of 3.2 M GdmCl	This paper	BMRB: 27701
Backbone 1H, 13C, and 15N Chemical Shift Assignments for the Myc bHLH-LZ domain in presence of 2.4 M GdmCl	This paper	BMRB: 27702
Backbone 1H, 13C, and 15N Chemical Shift Assignments for the Myc bHLH-LZ domain in presence of 1.6 M GdmCl.	This paper	BMRB: 27703
Backbone 1H, 13C, and 15N Chemical Shift Assignments for the Myc bHLH-LZ domain	This paper	BMRB: 27704
Crystal structure of Myc-Max recognizing	(Nair and Burley, 2003)	PDB 1nkp
Structural ensemble of Myc bHLH-LZ domain consistent with NMR data	This paper	DOI: 10.17632/xhdwd26fd c.1
Backbone 1H, 15N Chemical Shift Assignments for the Myc bHLH-LZ domain as a function of GdmCl concentration.	This paper	DOI: 10.17632/xhdwd26fd c.1
Backbone 1H, 15N Chemical Shift Assignments for the Myc bHLH-LZ domain as a function of NaCl concentration.	This paper	DOI:10.17632/xhdw d26fdc.1
PREs as used in structure model selection	This paper	DOI: 10.17632/xhdwd26fd c.1
Backbone 1H, 13C, 15N Chemical Shift Assignments for the Myc bHLH-LZ domain as used in structure model selection	This paper	DOI: 10.17632/xhdwd26fd c.1
PREs for 3 variants (365-SL, 386-SL and 405-SL) as a function of GdmCl concentration.	This paper	DOI: 10.17632/xhdwd26fd c.1
Experimental Models: Organisms/Strains		
Oligonucleotides		
Recombinant DNA		
6xHis-Tagged-Myc-351-437	This paper	N/A
Software and Algorithms		

Topspin 3.5	Bruker	N/A
CCPN Analysis 2.3	CCPN	N/A
Numeric python routines		N/A
Flexible Meccano	Ozenne <i>et al.</i> 2012	N/A
Asteroids	Salmon <i>et al.</i> 2010	N/A
SPARTA	Chen & Bax 2007	N/A
Other		

References

Babu, M.M., van der Lee, R., de Groot, N.S., and Gsponer, J. (2011). Intrinsically disordered proteins: regulation and disease. *Current Opinion in Structural Biology* 21, 432-440.

Baldwin, A.J., and Kay, L.E. (2009). NMR spectroscopy brings invisible protein states into focus. *Nature Chemical Biology* 5, 808-814.

Beaulieu, M.E., McDuff, F.O., Frappier, V., Montagne, M., Naud, J.F., and Lavigne, P. (2012). New structural determinants for c-Myc specific heterodimerization with Max and development of a novel homodimeric c-Myc b-HLH-LZ. *Journal of molecular recognition : JMR* 25, 414-426.

Bermel, W., Bertini, I., Chill, J., Felli, I., Haba, N., Kumar, M., and Pierattelli, R. (2012). Exclusively heteronuclear (13) C-detected amino-acid-selective NMR experiments for the study of intrinsically disordered proteins (IDPs). *ChemBiochem* 13, 2425-2432.

Bertoncini, C.W., Jung, Y.-S., Fernandez, C.O., Hoyer, W., Griesinger, C., Jovin, T.M., and Zweckstetter, M. (2005). Release of long-range tertiary interactions potentiates aggregation of natively unstructured α -synuclein. *Proceedings of the National Academy of Sciences of the United States of America* 102, 1430-1435.

1 Bhowmick, A., Brookes, D.H., Yost, S.R., Dyson, H.J., Forman-Kay, J.D., Gunter, D., Head-
2 Gordon, M., Hura, G.L., Pande, V.S., Wemmer, D.E., *et al.* (2017). Finding our way in the dark
3 proteome. *Journal of the American Chemical Society* *138*, 9730-9742.
4
5 Blackwood, E.M., and Eisenman, R.N. (1991). Max: a helix-loop-helix zipper protein that
6 forms a sequence-specific DNA-binding complex with Myc. *Science* *251*, 1211.
7
8 Burton, R.A., Mattila, S., Taparowsky, E.J., and Post, C.B. (2006). B-Myc: N-Terminal
9 Recognition of Myc Binding Proteins. *Biochemistry* *45*, 9857-9865.
10
11 Candotti, M., Esteban-Martín, S., Salvatella, X., and Orozco, M. (2013). Toward an atomistic
12 description of the urea-denatured state of proteins. *Proc Natl Acad Sci U S A* *110*, 5933-5938.
13
14 Clarke, A.R., and Waltho, J.P. (1997). Protein folding pathways and intermediates. *Current*
15 *Opinion in Biotechnology* *8*, 400-410.
16
17 Cliff, M.J., Craven, C.J., Marston, J.P., Hounslow, A.M., Clarke, A.R., and Waltho, J.P.
18 (2009). The Denatured State of N-PGK Is Compact and Predominantly Disordered. *Journal of*
19 *Molecular Biology* *385*, 266-277.
20
21 Clore, G.M. (2013). Generating accurate contact maps of transient long-range interactions in
22 intrinsically disordered proteins by paramagnetic relaxation enhancement. *Biophys J*, *104*,
23 1635-1636.
24
25 Dedmon, M.M., Lindorff-Larsen, K., Christodoulou, J., Vendruscolo, M., and Dobson, C.M.
26 (2005). Mapping Long-Range Interactions in α -Synuclein using Spin-Label NMR and
27 Ensemble Molecular Dynamics Simulations. *Journal of the American Chemical Society* *127*,
28 476-477.
29
30 Fieber, W., Schneider, M.L., Matt, T., Krautler, B., Konrat, R., and Bister, K. (2001). Structure,
31 Function, and Dynamics of the Dimerization and DNA-binding Domain of Oncogenic
32 Transcription Factor v-Myc. *J Mol Biol* *307*, 1395-1410.
33
34
35
36
37
38
39
40
41
42
43
44
45
46
47
48
49
50
51
52
53
54
55
56
57
58
59
60
61
62
63
64
65

1 Follis, A.V., Hammoudeh, D.I., Daab, A., and Metallo, S.J. (2009). Small-molecule
2 perturbation of competing interactions between c-Myc and Max. *Bioorg Med Chem Lett* *19*,
3 807-810.
4
5 Follis, A.V., Hammoudeh, D.I., wang, H., Prochownik, E.V., and Metallo, S.J. (2008).
6 Structural rationale for the coupled binding and unfolding of the c-Myc oncoprotein by small
7 molecules. *Chemical Biology* *15*, 1149-1155.
8
9 Goradia, N., Wiedemann, C., Herbst, C., Görlach, M., Heinemann, S.H., Ohlenschläger, O.,
10 and Ramachandran, R. (2015). An approach to NMR assignment of intrinsically disordered
11 proteins. *Chemphyschem* *16*, 739-746.
12
13 Habchi, J., Tompa, P., Longhi, S., and Uversky, V.N. (2014). Introducing protein intrinsic
14 disorder. *Chemical Reviews* *114*, 6561–6588.
15
16 Hammoudeh, D.I., Follis, A.V., Prochownik, E.V., and Metallo, S.J. (2009). Multiple
17 Independent Binding Sites for Small-Molecule Inhibitors on the Oncoprotein c-Myc. *Journal of*
18 *the American Chemical Society* *131*, 7390-7401.
19
20 Harvey, S.R., Porrini, M., Stachl, C., MacMillan, D., Zinzalla, G., and Barran, P.E. (2012).
21 Small-Molecule Inhibition of c-MYC:MAX Leucine Zipper Formation Is Revealed by Ion
22 Mobility Mass Spectrometry. *J Am Chem Soc* *134*, 19384–19392.
23
24 Heller, G.T., Aprile, F.A., Bonomi, M., Camilloni, C., De Simone, A., and Vendruscolo, M.
25 (2017). Sequence Specificity in the Entropy-Driven Binding of a Small Molecule and a
26 Disordered Peptide. *Journal of Molecular Biology* *429*, 2772-2779.
27
28 Huang, J.-r., Gabel, F., Jensen, M.R., Grzesiek, S., and Blackledge, M. (2012). Sequence-
29 Specific Mapping of the Interaction between Urea and Unfolded Ubiquitin from Ensemble
30 Analysis of NMR and Small Angle Scattering Data. *Journal of the American Chemical Society*
31 *134*, 4429-4436.
32
33
34
35
36
37
38
39
40
41
42
43
44
45
46
47
48
49
50
51
52
53
54
55
56
57
58
59
60
61
62
63
64
65

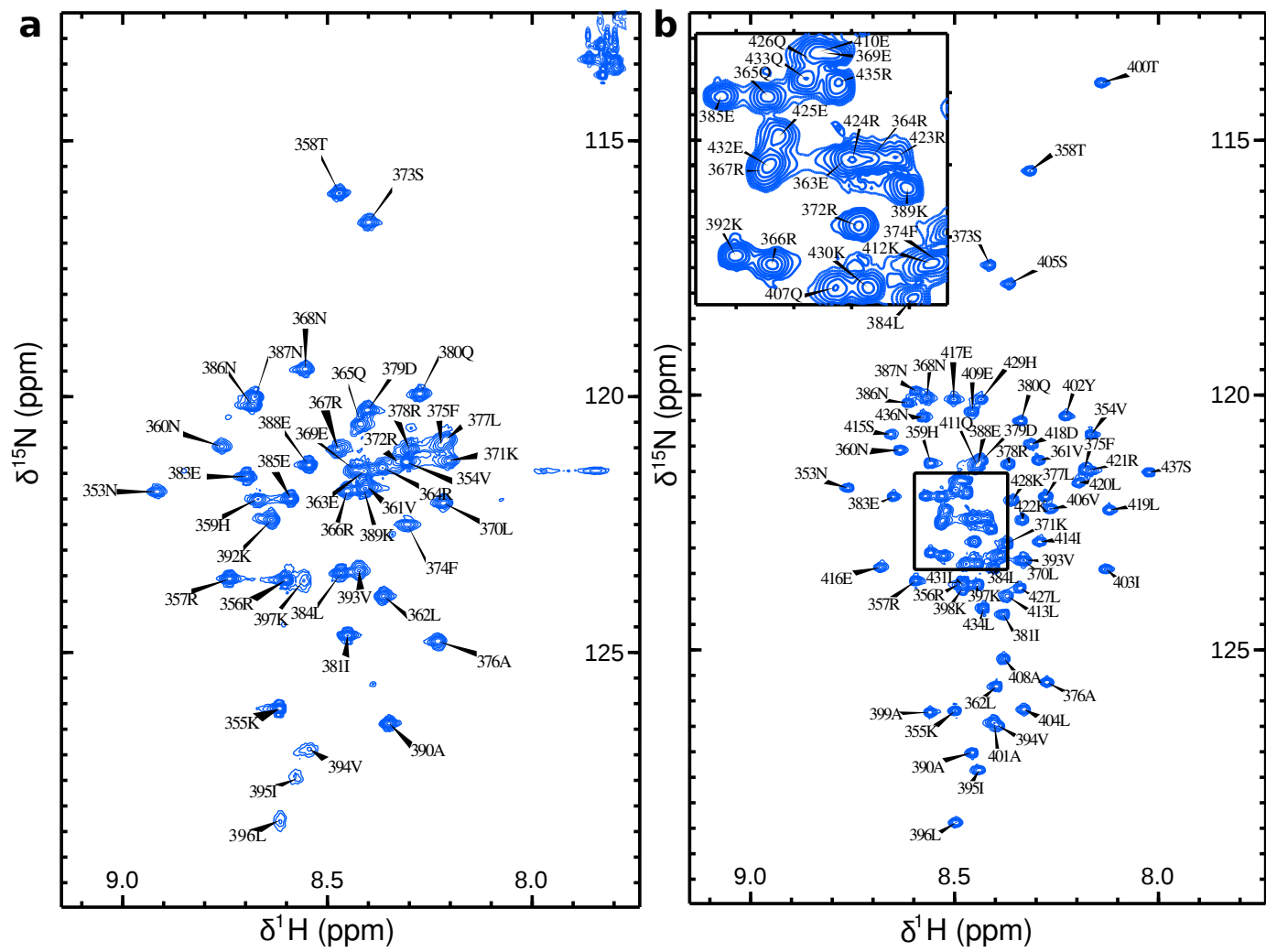
1 Jensen, M.R., Zwecksteter, M., Huang, J.-R., and Blackledge, M. (2014). Exploring Free-
2 Energy Landscapes of Intrinsically Disordered Proteins at Atomic Resolution Using NMR
3 Spectroscopy. *Chemical Reviews* *114*, 6632-6660.
4
5 Lavigne, P., Crump, M.P., Gagné, S.M., Hodges, R.S., Kay, C.M., and Sykes, B.D. (1998).
6 Insights into the mechanism of heterodimerization from the 1H-NMR solution structure of the
7 c-Myc-Max heterodimeric leucine zipper11Edited by P. E. Wright. *Journal of Molecular*
8 *Biology* *281*, 165-181.
9
10 Liu, J., Dai, J., He, J., Niemi, A.J., and Ilieva, N. (2017). Multistage modeling of protein
11 dynamics with monomeric Myc oncoprotein as an example. *Phys Rev E* *95*, 032406.
12
13 Macek, P., Cliff, M.J., Embrey, K.J., Holdgate, G.A., Nissink, W.M., Panova, S., Waltho, J.P.,
14 and Davies, R.A. (2018). Myc phosphorylation in its basic helix–loop–helix region
15 destabilizes transient α -helical structures, disrupting Max
16 and DNA binding (*in press*). *J Biol Chem* *293*, -.
17
18 Marsh, J.A., Neale, C., Jack, F.E., Choy, W.Y., Lee, A.Y., Crowhurst, K.A., and Forman-Kay,
19 J.D. (2007). Improved structural characterizations of the drkN SH3 domain unfolded state
20 suggest a compact ensemble with native-like and non-native structure. *Journal of Molecular*
21 *Biology* *367*, 1494-1510.
22
23 McParland, V.J., Kalverda, A.P., Homans, S.W., and Radford, S.E. (2002). Structural
24 properties of an amyloid precursor of β 2-microglobulin. *Nature Structural Biology* *9*, 326.
25
26 Meier, S., Grzesiek, S., and Blackledge, M. (2007). Mapping the conformational landscape of
27 urea-denatured ubiquitin using residual dipolar couplings. *Journal of the American Chemical*
28 *Society* *129*, 9799-9807.
29
30 Metallo, S.J. (2010). Intrinsically disordered proteins are potential drug targets. *Current*
31 *Opinion in Chemical Biology* *14*, 481–488.

1 Milanese, L., Waltho, J.P., Hunter, C.A., Shaw, D.J., Beddard, G.S., Reid, G.D., Dev, S., and
2 Volk, M. (2012). Measurement of energy landscape roughness of folded and unfolded proteins.
3
4
5 3 Proceedings of the National Academy of Sciences *109*, 19563.
6
7 4 Myers, J.K., Pace, C.N., and Scholtz, J.M. (1995). Denaturant m values and heat capacity
8
9
10 5 changes: relation to changes in accessible surface areas of protein unfolding. Protein science : a
11
12 6 publication of the Protein Society *4*, 2138-2148.
13
14 7 Nair, S.K., and Burley, S.K. (2003). X-Ray Structures of Myc-Max and Mad-Max Recognizing
15
16
17 8 DNA: Molecular Bases of Regulation by Proto-Oncogenic Transcription Factors. Cell *112*,
18
19 9 193-205.
20
21
22 10 Oldfield, C.J., and Dunker, A.K. (2014). Intrinsically disordered proteins and intrinsically
23
24 11 disordered protein regions. Annu Rev Biochem *83*, 553-584.
25
26
27 12 Ozenne, V., Schneider, R., Yao, M.X., Huang, J.R., Salmon, L., Zweckstetter, M., Jensen,
28
29 13 M.R., and Blackledge, M. (2012). Mapping the Potential Energy Landscape of Intrinsically
30
31
32 14 Disordered Proteins at Amino Acid Resolution. Journal of the American Chemical Society *134*,
33
34 15 15138-15148.
35
36
37 16 Plaxco, K.W., Morton, C.J., Grimshaw, S.B., Jones, J.A., Pitkeathly, M., Campbell, I.D., and
38
39 17 Dobson, C.M. (1997). The effects of guanidine hydrochloride on the 'random coil'
40
41 18 conformations and NMR chemical shifts of the peptide series GGXGG. J Biomol NMR *10*,
42
43
44 19 221-230.
45
46 20 Prendergast, G.C., Lawe, D., and Ziff, E.B. (1991). Association of Myn, the murine homolog of
47
48
49 21 Max, with c-Myc stimulates methylation-sensitive DNA binding and ras cotransformation. Cell
50
51 22 *65*, 395-407.
52
53
54 23 Reed, M.A.C., Jelinska, C., Syson, K., Cliff, M.J., Splevins, A., Alizadeh, T., Hounslow, A.M.,
55
56 24 Staniforth, R.A., Clarke, A.R., Craven, C.J., *et al.* (2006). The denatured state under native

1 conditions: A non-native-like collapsed state of N-PGK. *Journal of Molecular Biology* 357,
2 365-372.
3
4 3 Salmon, L., Nodet, G., Ozenne, V., Yin, G., Jensen, M.R., Zweckstetter, M., and Blackledge,
5 M. (2010). NMR characterization of long-range order in intrinsically disordered proteins.
6
7 4 *Journal of the American Chemical Society* 132, 8407-8418.
8
9 5
10 6 Santarius, T., Shipley, J., Brewer, D., Stratton, M.R., and Cooper, C.S. (2010). A census of
11
12 7 amplified and overexpressed human cancer genes. *Nat Rev Cancer* 10, 59-64.
13
14 8 Scholtz, J.M., Grimsley, G.R., and Pace, C.N. (2009). SOLVENT DENATURATION OF
15
16 9 PROTEINS AND INTERPRETATIONS OF THE M VALUE. In *Methods in Enzymology*,
17
18 10 Vol 466: Biothermodynamics, Pt B, M.L. Johnson, J.M. Holt, and G.K. Ackers, eds., pp. 549-
19
20 11 565.
21
22 12 Schulman, B.A., Kim, P.S., Dobson, C.M., and Redfield, C. (1997). A residue-specific NMR
23
24 13 view of the non-cooperative unfolding of a molten globule. *Nat Struct Biol* 4, 630-634.
25
26 14 Schwalbe, M., Ozenne, V., Bibow, S., Jaremko, M., Jaremko, L., Gajda, M., Jensen, Malene R.,
27
28 15 Biernat, J., Becker, S., Mandelkow, E., *et al.* (2014). Predictive Atomic Resolution
29
30 16 Descriptions of Intrinsically Disordered hTau40 and α -Synuclein in Solution from NMR and
31
32 17 Small Angle Scattering. *Structure* 22, 238-249.
33
34 18 Shen, Y., and Bax, A. (2007). Protein backbone chemical shifts predicted from searching a
35
36 19 database for torsion angle and sequence homology. *J Biomol NMR* 38, 289-302.
37
38 20 Sormanni, P., Piovesan, D., Heller, G., Bonomi, M., Kukic, P., Camilloni, C., Fuxreiter, M.,
39
40 21 Dosztanyi, Z., Pappu, R., Babu, M.M., *et al.* (2017). Simultaneous quantification of protein
41
42 22 order and disorder. *Nature Chemical Biology* 13, 339-342.
43
44 23 Soucek, L., Helmer-Citterich, M., Sacco, A., Jucker, R., Cesareni, G., and Nasi, S. (1998).
45
46 24 Design and properties of a myc derivative that efficiently homodimerizes. *Oncogene* 17, 2463-
47
48 25 2472.
49
50
51
52
53
54
55
56
57
58
59
60
61
62
63
64
65

1 van der Lee, R., Buljan, M., Lang, B., Weatheritt, R.J., Daughdrill, G.W., Dunker, A.K.,
2 Fuxreiter, M., Gough, J., Gsponer, J., Jones, D.T., *et al.* (2014). Classification of Intrinsically
3 Disordered Regions and Proteins. *Chemical Reviews* 114, 6589-6631.
4
5 Wiedemann, C., Goradia, N., Häfner, S., Herbst, C., Görlach, M., Ohlenschläger, O., and
6 Ramachandran, R. (2015). HN-NCA heteronuclear TOCSY-NH experiment for (1)H(N) and
7 (15)N sequential correlations in ((13)C, (15)N) labelled intrinsically disordered proteins. *J*
8 *Biomol NMR* 63, 201-212.
9
10 Wright, P.E., and Dyson, H.J. (2015). Intrinsically disordered proteins in cellular signalling and
11 regulation. *Nat Rev Mol Cell Biol* 16, 18-29.
12
13 Yin, X., Giap, C., Lazo, J.S., and Prochownik, E.V. (2003). Low molecular weight inhibitors of
14 Myc–Max interaction and function. *Oncogene* 22, 6151.
15
16 Zhang, O.W., Kay, L.E., Shortle, D., and FormanKay, J.D. (1997). Comprehensive NOE
17 characterization of a partially folded large fragment of staphylococcal nuclease Delta 131
18 Delta, using NMR methods with improved resolution. *Journal of Molecular Biology* 272, 9-20.
19
20
21
22
23
24
25
26
27
28
29
30
31
32
33
34
35
36
37
38
39
40
41
42
43
44
45
46
47
48
49
50
51
52
53
54
55
56
57
58
59
60
61
62
63
64
65

Figure 1



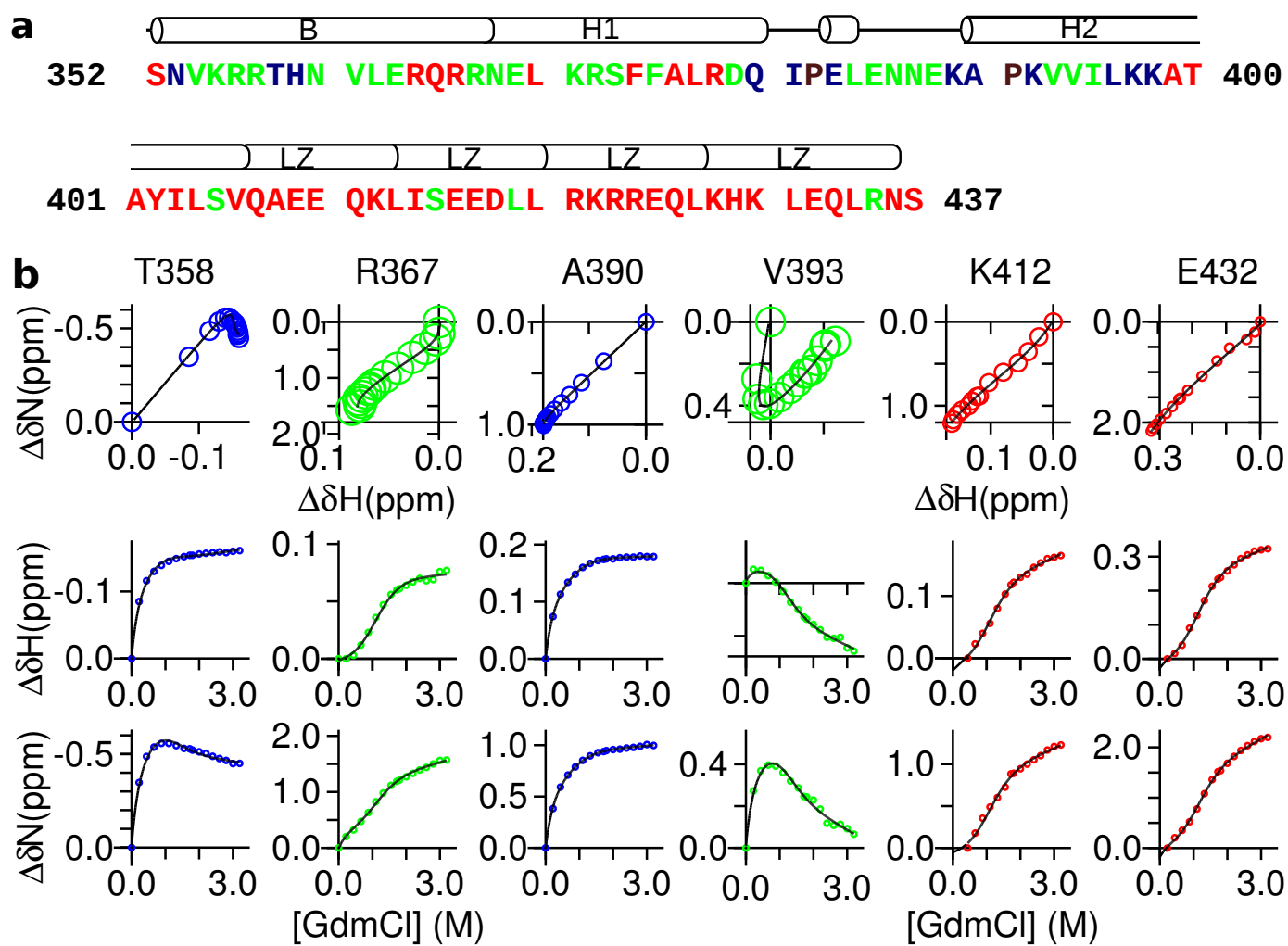


Figure 3

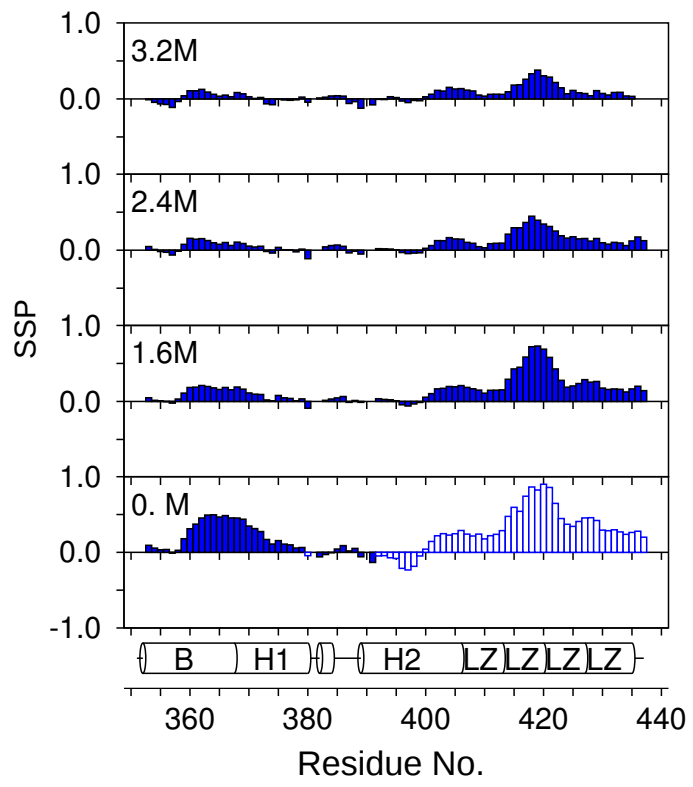


Figure 4

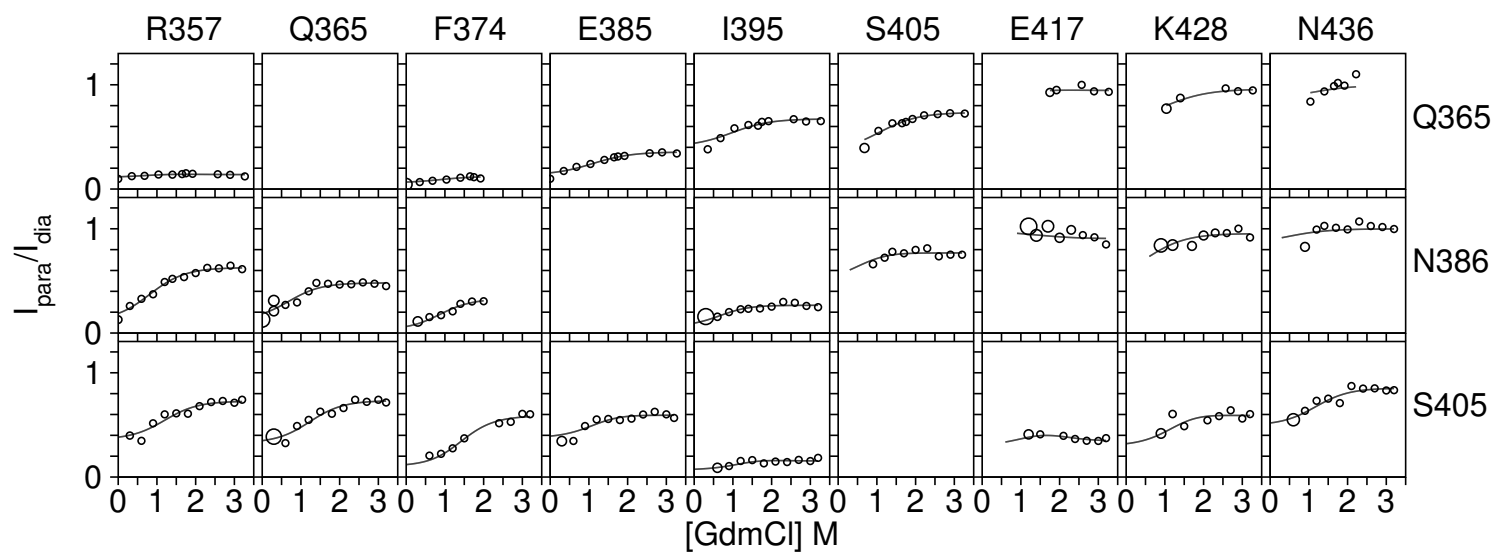


Figure 5

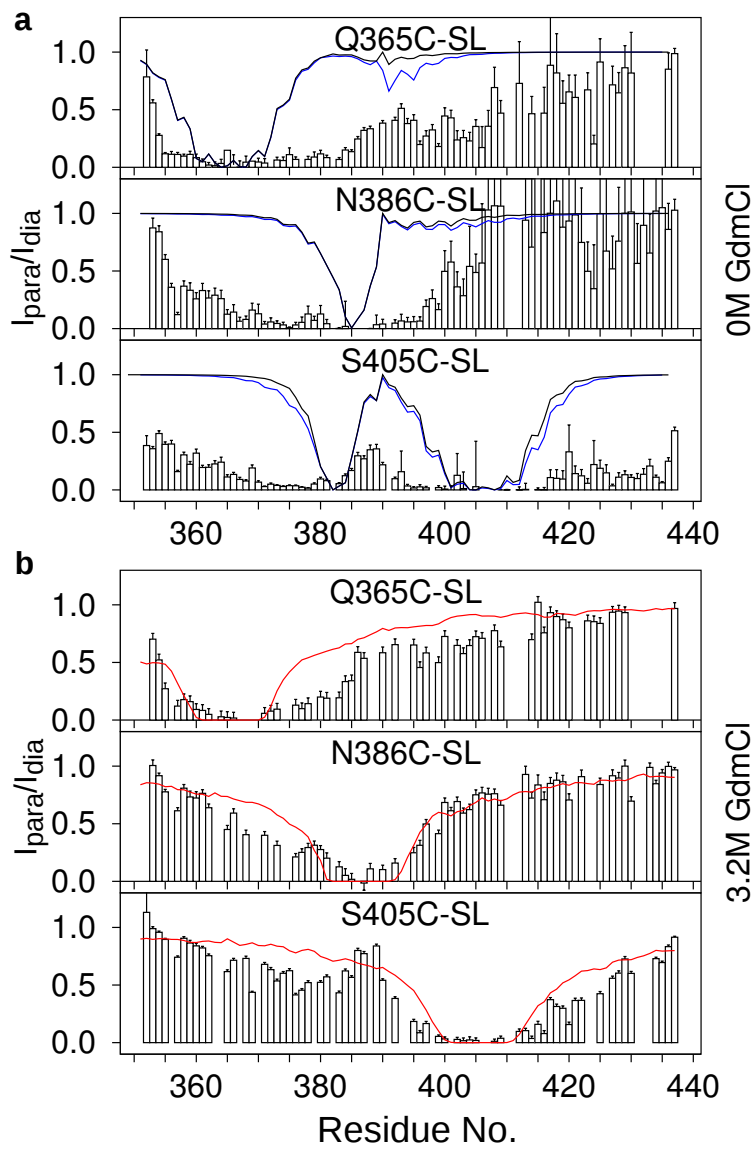


Figure 6

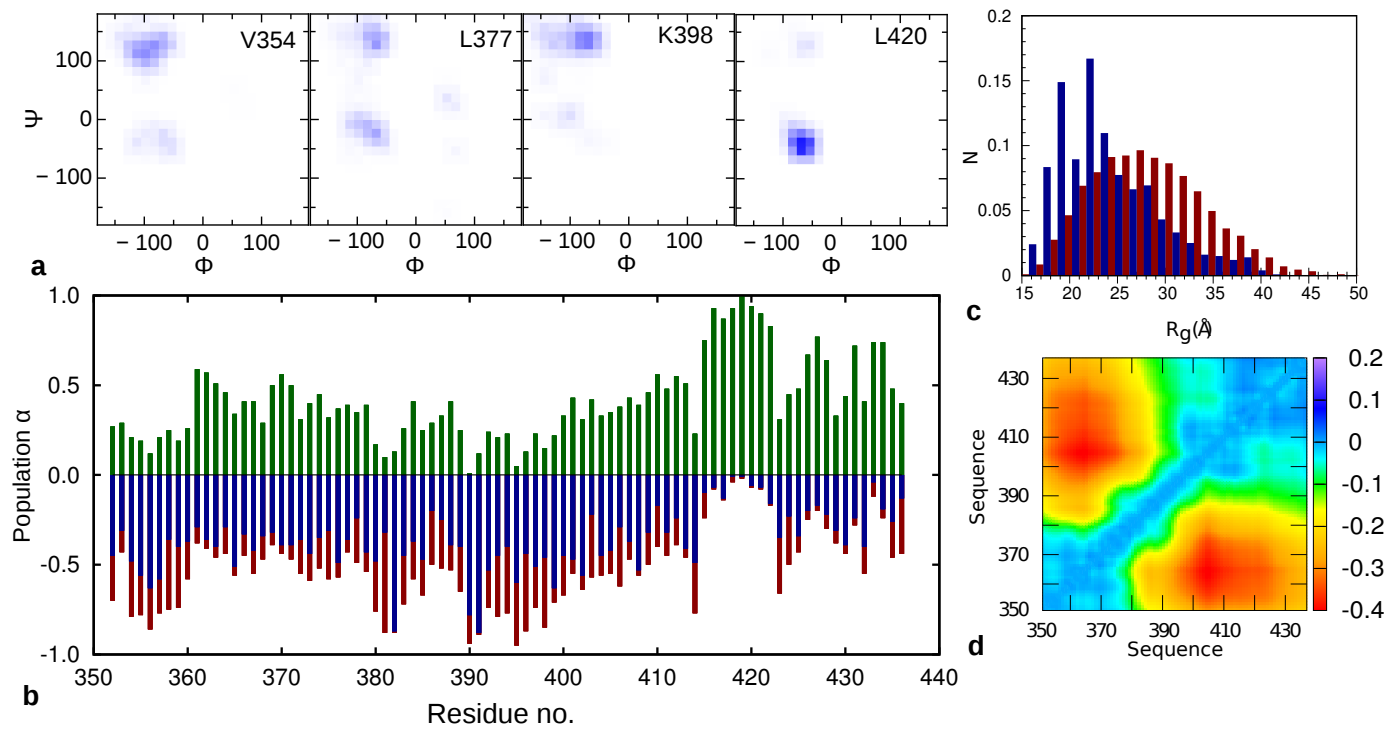


Figure 7

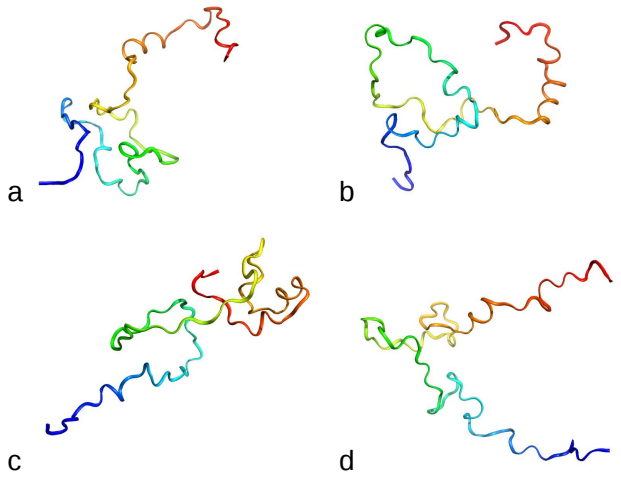
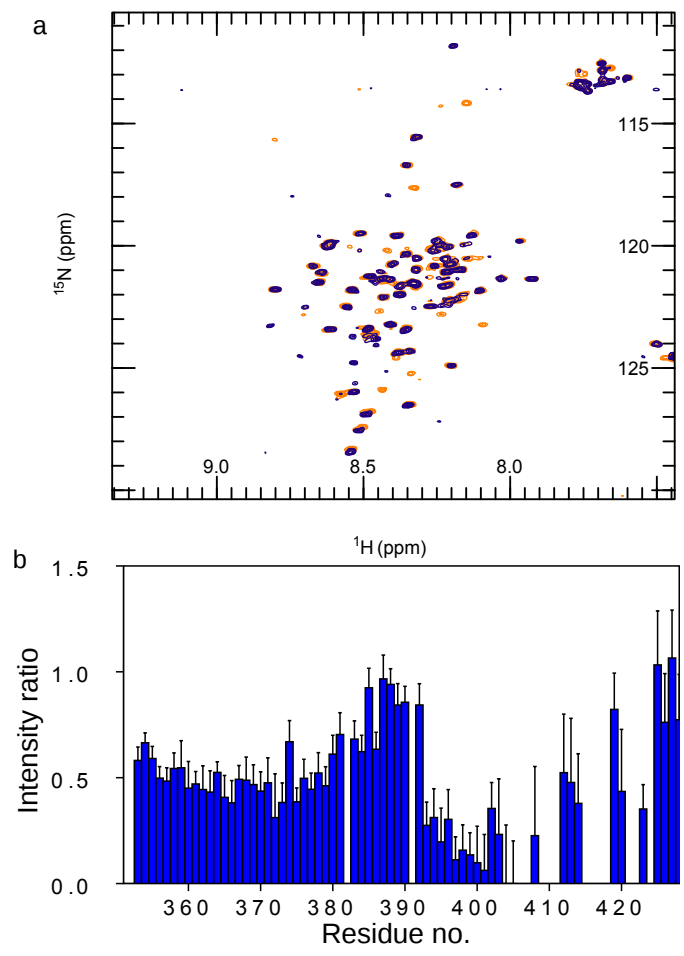


Figure 8



Supplemental Data

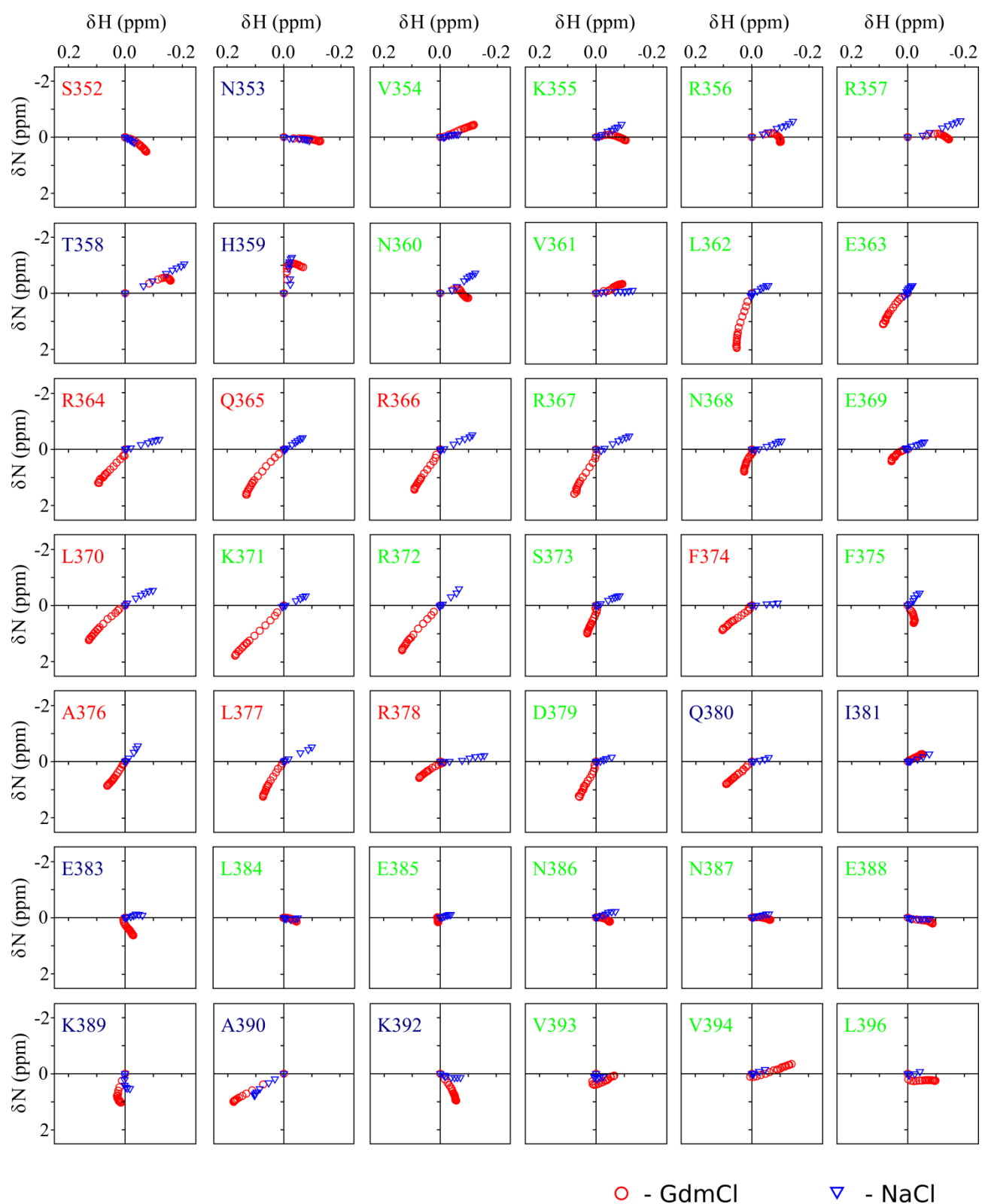


Figure S1: (relates to Fig. 2) The behaviour of observable ^1H , ^{15}N correlation peaks in HSQC spectra of Myc over a GdmCl titration and a NaCl titration. GdmCl concentration range (red circles): 0.0 to 3.2 M, with 0.2 M steps. NaCl concentration range (blue triangles): 0.0 to 1.2 M, with 0.2 M steps. Residue names are coloured as in Fig. 1.

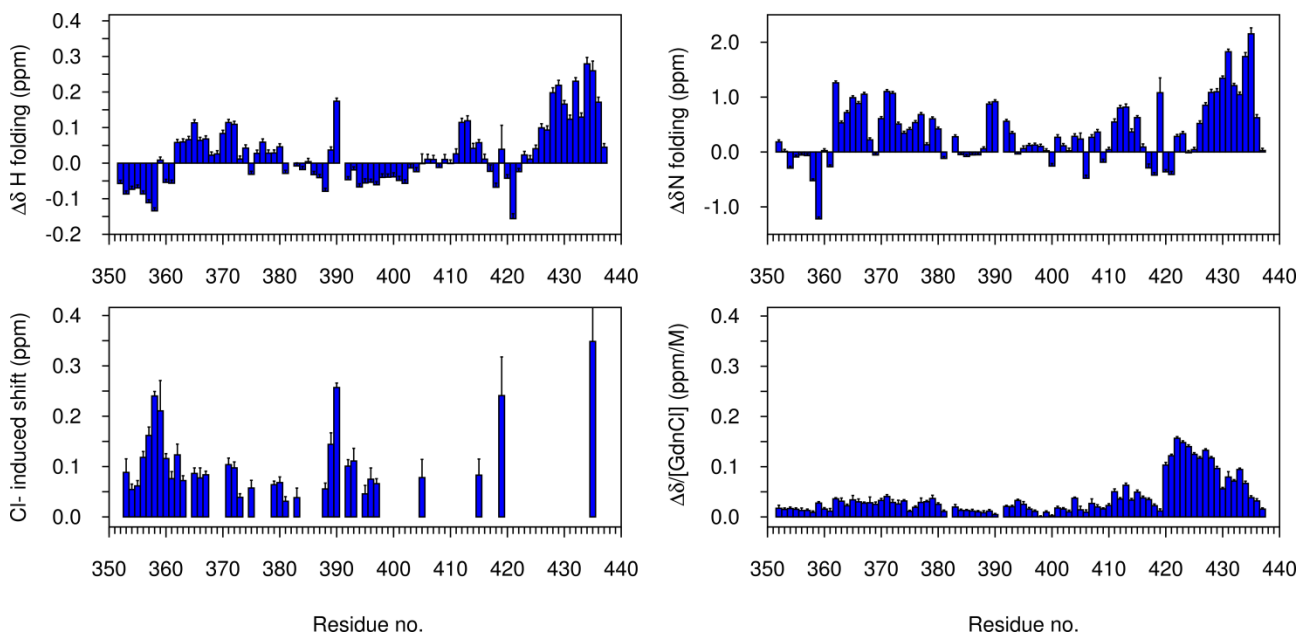


Figure S2 Relates to **Fig 2**. Values of best fit residue-specific parameters for proton (top-left) and nitrogen (top-right) chemical shift for the sigmoidal transition ($\Delta\delta H_{\text{folding}}$ and $\Delta\delta N_{\text{folding}}$), the Cl⁻ induced hyperbolic transition (expressed as $((\Delta\delta H_{\text{Cl}})^2 + (\Delta\delta N_{\text{Cl}}/6)^2)^{0.5}$, bottom-left) and the slope of final shallow transition (bottom-right).

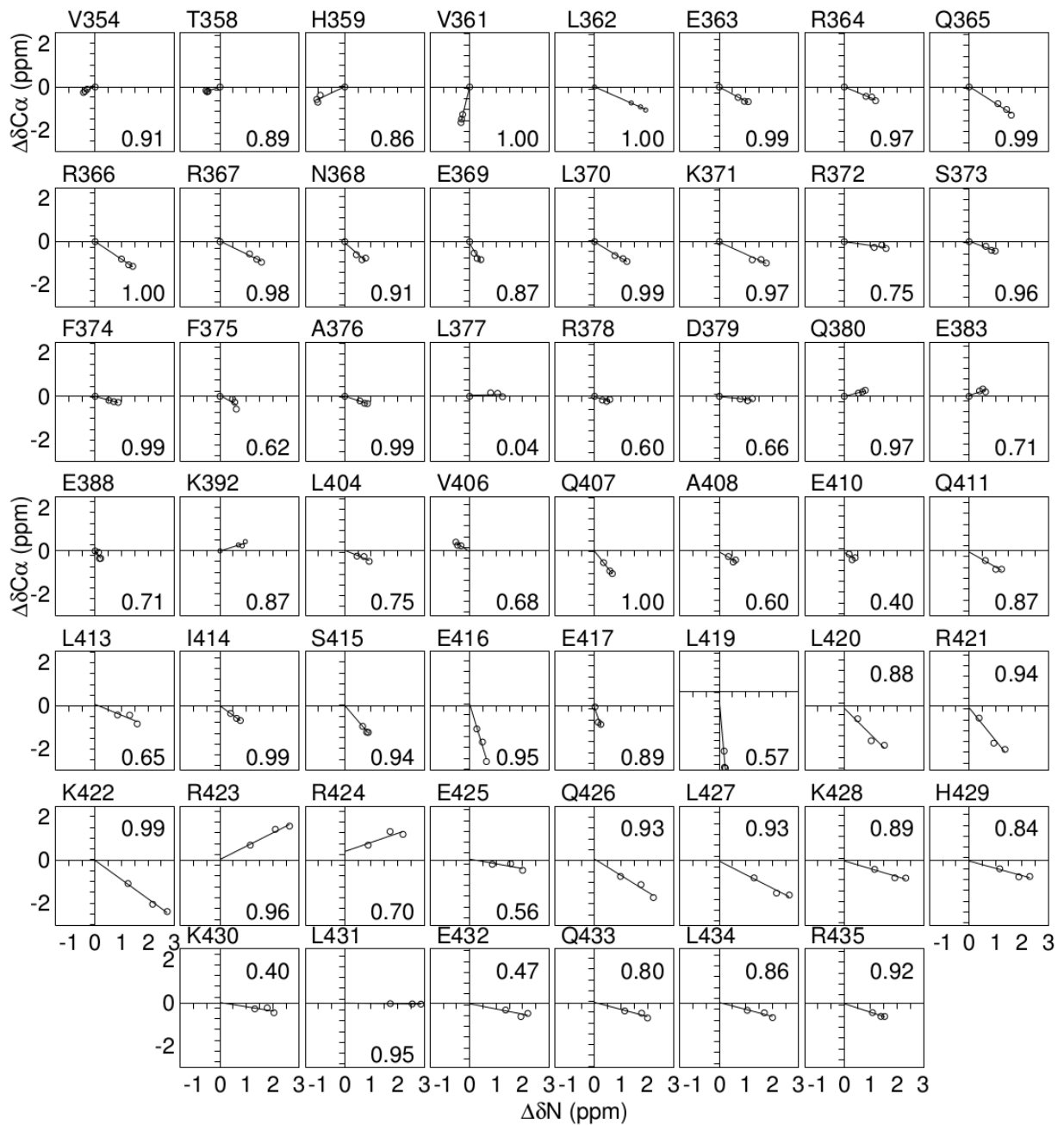


Figure S3: relates to **Fig. 3**, δC_{α} plotted against $\Delta \delta N$ for representative residues. Correlation coefficients are shown inset for each residue.

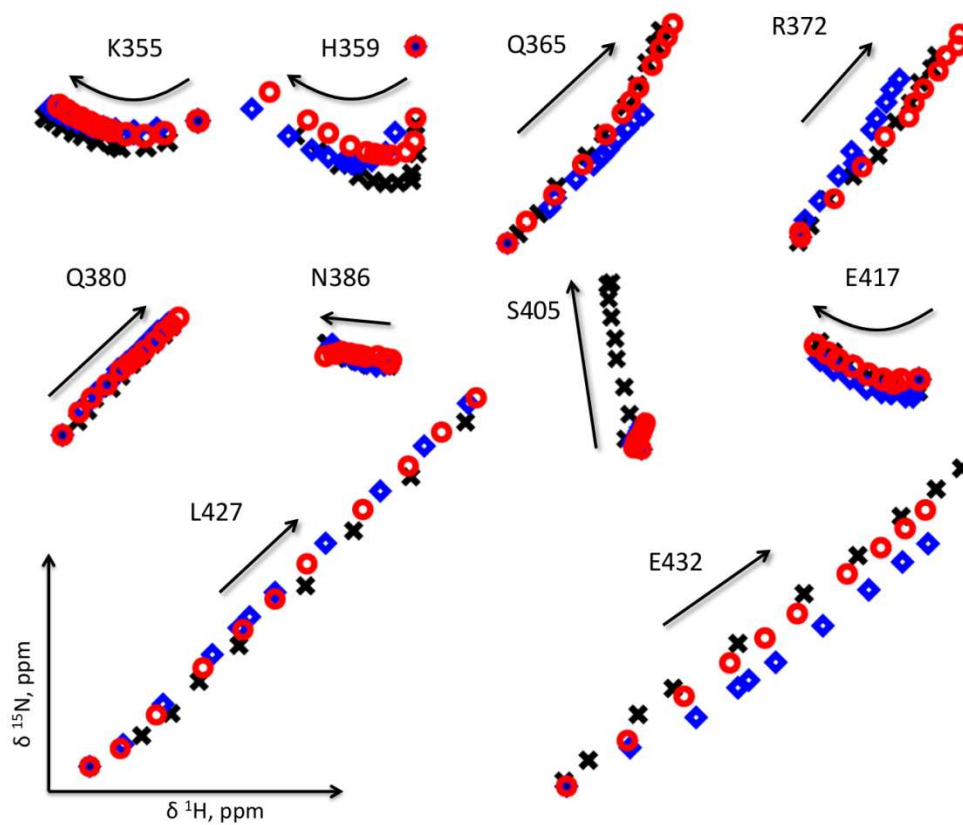


Figure S4: relates to **Fig. 4**. Denaturation profiles mapped as cross-peaks from ^1H - ^{15}N HSQC spectra for the different Myc cysteine mutants: Q365C (blue diamonds), N386 (red circles), S405 (black crosses). The radii of the circles (dimensions of crosses and squares) correspond to 0.015 ppm in the ^1H dimension HSQC spectra. Arrows point in the direction of the cross-peak motion upon increasing GdmCl concentration.

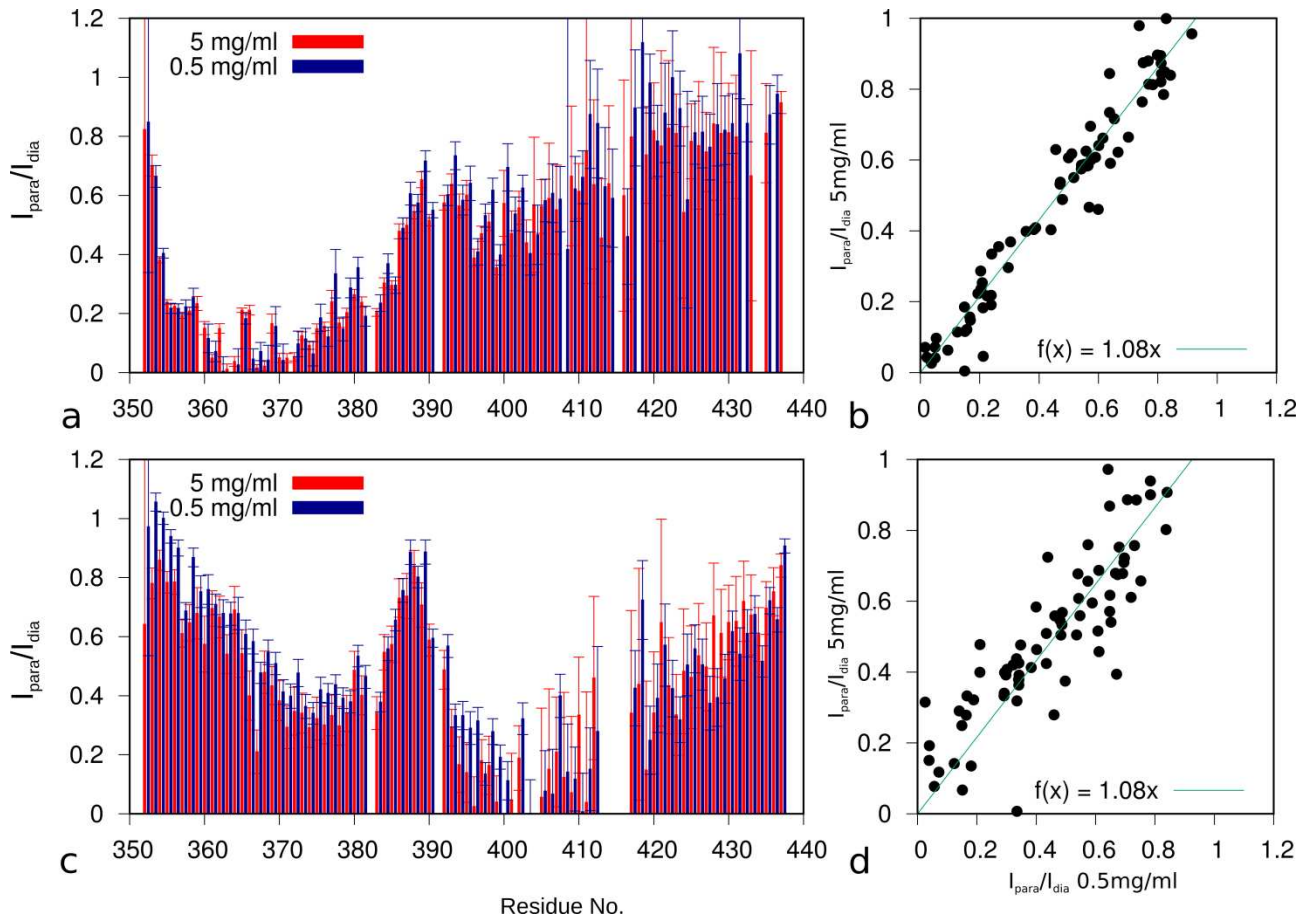


Figure S5: relates to **Fig 5**. Sequence distribution of PREs (I_{para}/I_{dia}) at 0.5 (blue) and 5 (red) mg/ml at 0.6 M GdmCl, for Q365C (A) and S405C (C) spin-labelled variants. PRE ratios of 0.5 mg/ml vs 5 mg/ml were plotted to illustrate correlation between them (B and D) and regression coefficient (slope value).

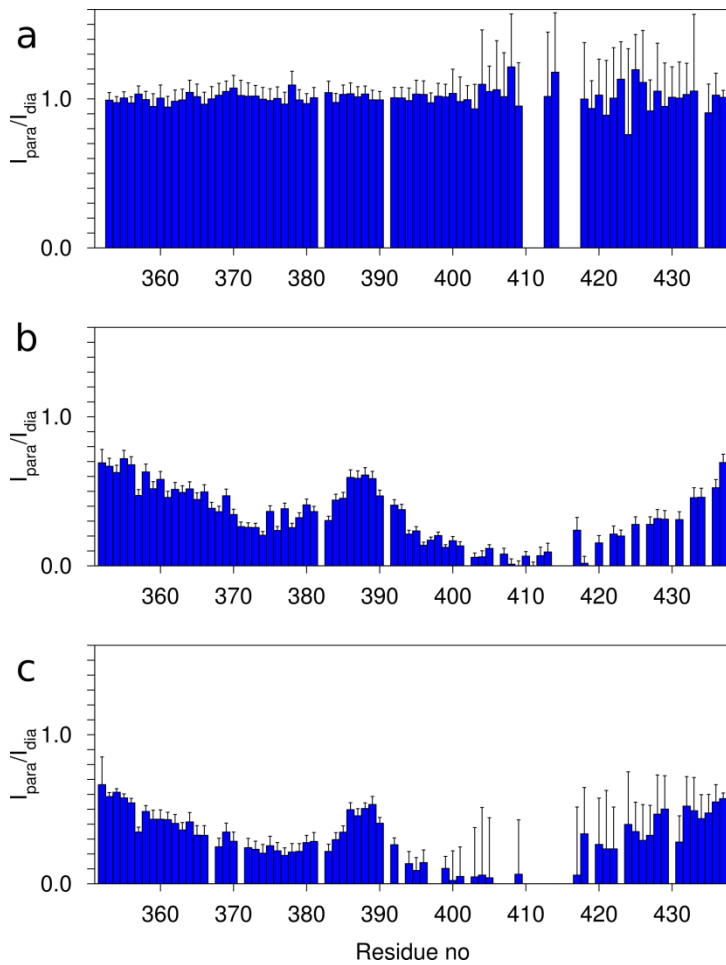
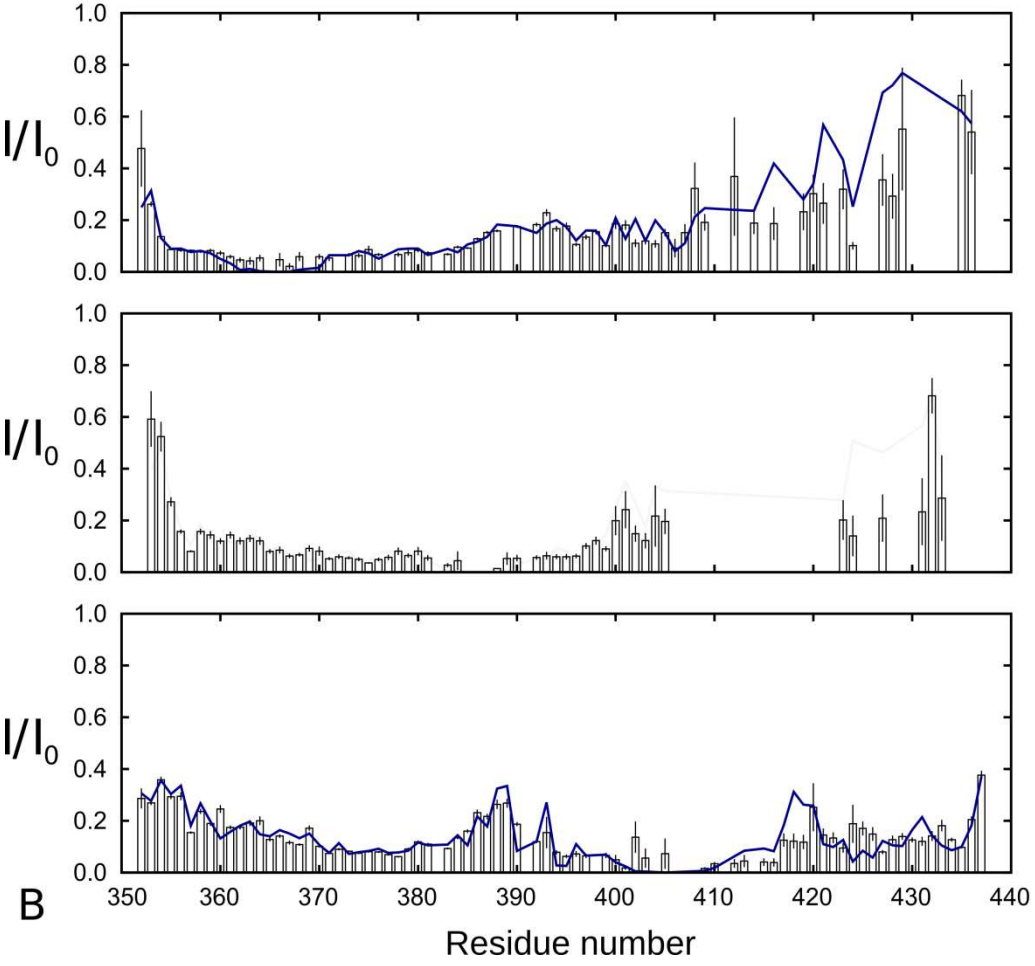
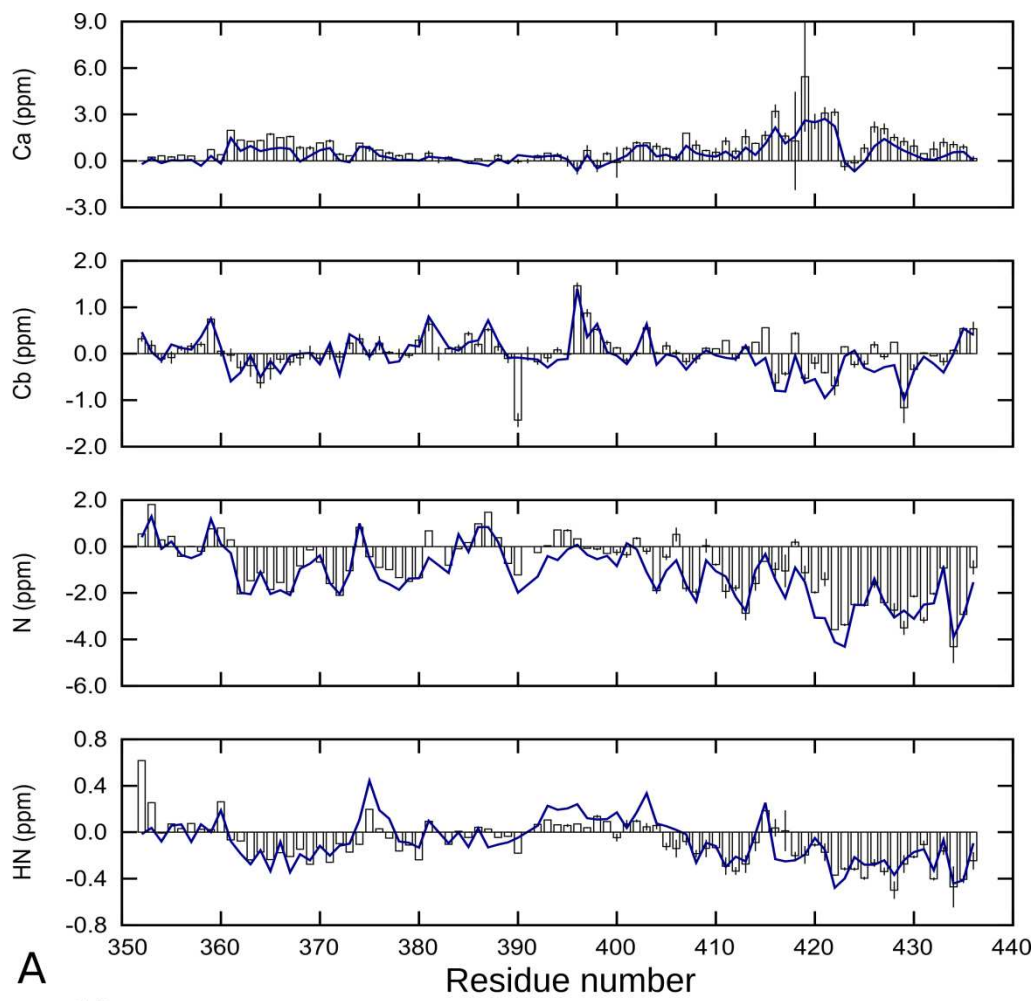


Figure S6: Relates to **Fig. 5**. Intensity ratios of samples with paramagnetic MTSL to diamagnetic MTSL when **a)** ^{14}N -Myc Q411-MTSL is in 1:1 mix with underivatized ^{15}N Myc Q411 at 4 mg/ml **b)** ^{15}N -Myc Q411-MTSL at the same concentration. **c)** ^{15}N -Myc S405-MTSL at the same concentration

1
2
3
4
5
6
7
8
9
10
11
12
13
14
15
16
17
18
19
20
21
22
23
24
25
26
27
28
29
30
31
32
33
34
35
36
37
38
39
40
41
42
43
44
45
46
47
48
49
50
51
52
53
54
55
56
57
58
59
60
61
62
63
64
65



1
2 **Figure S7:** Relates to **Fig. 6 & 7.** Comparison of the experimental (empty bars) and ensemble
3 averaged data (blue line) for Myc at 0 M GdmCl. (A) Chemical shift deviation from random coil values
4 back-calculated by SPARTA; (B) Intensity ratios between paramagnetic and diamagnetic samples on a
5 per residue level.
6
7
8
9
10
11
12
13
14
15
16
17
18
19
20
21
22
23
24
25
26
27
28
29
30
31
32
33
34
35
36
37
38
39
40
41
42
43
44
45
46
47
48
49
50
51
52
53
54
55
56
57
58
59
60
61
62
63
64
65